energies

MDPI

Article

Near-Infrared Spectroscopy Modeling of Combustion Characteristics in Chip and Ground Biomass from Fast-Growing Trees and Agricultural Residue

Bijendra Shrestha [1], Jetsada Posom [2], Pimpen Pornchaloempong [3], Panmanas Sirisomboon [1,*], Bim Prasad Shrestha [4,5,*] and Hidayah Ariffin [6,7]

1 Department of Agricultural Engineering, School of Engineering, King Mongkut's Institute of Technology Ladkrabang, Bangkok 10520, Thailand; 63601254@kmitl.ac.th
2 Department of Agricultural Engineering, Faculty of Engineering, Khon Kaen University, Khon Kaen 40002, Thailand; jetspo@kku.ac.th
3 Department of Food Engineering, School of Engineering, King Mongkut's Institute of Technology Ladkrabang, Bangkok 10520, Thailand; pimpen.po@kmitl.ac.th
4 Department of Mechanical Engineering, School of Engineering, Kathmandu University, Dhulikhel P.O. Box 6250, Nepal
5 Department of Bioengineering, University of Washington, William H. Foege Building 3720, 15th Ave. NE, Seattle, WA 98195-5061, USA
6 Department of Bioprocess Technology, Faculty of Biotechnology and Biomolecular Sciences, Universiti Putra Malaysia, Serdang 43400, Selangor, Malaysia; hidayah@upm.edu.my
7 Laboratory of Biopolymer and Derivatives, Institute of Tropical Forestry and Forest Products (INTROP), Universiti Putra Malaysia, Serdang 43400, Selangor, Malaysia
* Correspondence: panmanas.si@kmitl.ac.th (P.S.); shrestha@ku.edu.np (B.P.S.)

Abstract: This study focuses on the investigation and comparison of combustion characteristic parameters and combustion performance indices between fast-growing trees and agricultural residues as biomass sources. The investigation is conducted through direct combustion in an air environment using a thermogravimetric analyzer (TGA). Additionally, partial least squares regression (PLSR)-based models were developed to assess combustion performance indices via near-infrared spectroscopy (NIRS), serving as a non-destructive alternative method. The results obtained through the TGA reveal that, specifically, fast-growing trees display higher average ignition temperature (227 °C) and burnout temperature (521 °C) in comparison to agricultural residues, which exhibit the values of 218 °C and 515 °C, respectively. Therefore, fast-growing trees are comparatively difficult to ignite, but sustain combustion over extended periods, yielding higher temperatures. However, despite fast-growing trees having a high ignition index (D_i) and burnout index (D_f), the comprehensive combustion performance (S_i) and flammability index (C_i) of agricultural residue are higher, indicating the latter possess enhanced thermal and combustion reactivity, coupled with improved combustion stability. Five distinct PLSR-based models were developed using 115 biomass samples for both chip and ground forms, spanning the wavenumber range of 3595–12,489 cm^{-1}. The optimal model was selected by evaluating the coefficients of determination in the prediction set (R^2_P), root mean square error of prediction (RMSEP), and RPD values. The results suggest that the proposed model for D_f, obtained through GA-PLSR using the first derivative (D1), and S_i, achieved through full-PLSR with MSC, both in ground biomass, is usable for most applications, including research. The model yielded, respectively, an R^2_P, RMSEP, and RPD, which are 0.8426, 0.4968 wt.% min^{-4}, and 2.5; and 0.8808, 0.1566 wt.%^{2} min^{-2} °C^{-3}, and 3.1. The remaining models (D_i in chip and ground, D_f, and S_i in chip, and C_i in chip and ground biomass) are primarily applicable only for rough screening purposes. However, including more representative samples and exploring a more suitable machine learning algorithm are essential for updating the model to achieve a better nondestructive assessment of biomass combustion behavior.

check for updates

Citation: Shrestha, B.; Posom, J.; Pornchaloempong, P.; Sirisomboon, P.; Shrestha, B.P.; Ariffin, H. Near-Infrared Spectroscopy Modeling of Combustion Characteristics in Chip and Ground Biomass from Fast-Growing Trees and Agricultural Residue. *Energies* **2024**, *17*, 1338. https://doi.org/10.3390/en17061338

Academic Editor: Maria Founti

Received: 6 February 2024
Revised: 1 March 2024
Accepted: 6 March 2024
Published: 11 March 2024

Keywords: biomass; combustion; thermogravimetric analyzer; near-infrared spectroscopy; partial least squares regression

1. Introduction

Global energy demand continues to escalate, prompting the exploration of diverse energy sources to meet this growing need, while mitigating the negative impacts on both energy availability and the environment. The predominant reliance on non-renewable fossil fuels not only contributes to environmental degradation but also raises concerns about future energy security due to the finite reserves. According to the International Energy Agency, as of 2020, 80% of global primary energy consumption was attributed to fossil fuels, resulting in a substantial carbon footprint [1]. The financial burdens associated with fossil fuels, exacerbated by fluctuating prices and geopolitical uncertainties, have triggered an urgent quest for alternative energy options.

A balanced and sustainable energy portfolio necessitates the promotion of renewable energy sources, primarily including hydro, wind, solar, biomass, and geothermal. Among these, biomass energy stands out as a promising solution, which accounts for 15% of the total energy consumption [2], and is derived from continuously renewable organic materials, such as wood, agricultural residues, and organic waste. Biomass energy conversion occurs predominantly through direct combustion [3], thermochemical processes (specifically pyrolysis and gasification) to produce solid (charcoal) and gaseous (syngas) fuels, as well as biological methods involving fermentation to produce ethanol and anaerobic digestion to yield methane-rich biogas. The utilization of biomass for energy purposes not only reduces reliance on non-renewable sources but also aids in waste management, contributing to rural development.

The fulfillment of global primary energy relies on the direct combustion of biomass and the co-combustion of two or more different fuels within the same combustion system, such as biomass and biochar [4], textile dyeing sludge and waste rubber [5], phytoremediation biomass and textile dyeing sludge [6], calcium-rich oil shale with biomass [7]. Despite biomass being deemed a carbon-neutral fuel [8], it exhibits varied combustion behaviors [9]. Therefore, careful management of the combustion process is vital to minimize emissions of additional pollutants, including particulate matter, sulfur oxides (SO_x), nitrogen oxides (NO_x), and volatile organic compounds [10]. A thorough comprehension of the combustion properties across different types of biomass is imperative to appropriately choose suitable biomass and design efficient combustion systems. Hence, combustion characteristic parameters, such as biomass ignition time (t_i) and ignition temperature (T_i), burnout time (t_f) and burnout temperature (T_f), maximum and average combustion rate, etc., are essential for evaluating combustion performance indices such as the D_i, D_f, S_i, and C_i [11]. Accurate assessment of these indices can enhance the overall efficiency of the biomass combustion system, reduce environmental impacts, and bring us closer to achieving a sustainable energy future driven by renewable sources.

TGA is typically employed to determine combustion characteristic parameters for evaluating different combustion performance indices [12]. Biomass combustion in TGA mainly consists of three stages: (i) water evaporation, (ii) volatile release and its combustion, and (iii) char combustion [13–15]. TGA logs the mass loss of biomass as a function of time and temperature. As a result, the thermogravimetric (TG) curve obtained through TGA provides information about the mass loss of the biomass sample as it undergoes thermal decomposition and combustion. The DTG curve is derived as the D1 from the TG curves, providing additional information about the rate of mass loss at various times and temperatures [15]. Based on the TG and DTG curves, various combustion characteristic parameters can be identified. These parameters are used to evaluate the D_i, D_f, S_i, and C_i. TGA has been employed in a various range of studies, covering diverse aspects of combustion and thermal behavior. It has been used to assess the self-ignition potential of

woody biomass and wheat straw [2], investigate the thermal behavior of Malaysian oil palm biomass, low-rank coal, and their respective blends under oxidative atmosphere [16], and identify thermo-chemical characteristics data for date palm biomass [17]. TGA has also been instrumental in studying the ignition behavior of straw pellets [18] and investigating ignition and burnout in bamboo and sugarcane bagasse [19]. Furthermore, TGA has been utilized to analyze the combustion characteristics of various biomass pellet types, including rubberwood sawdust pellets, teak sawdust pellets, eucalyptus bark pellets, cassava rhizome pellets [20], as well as agricultural solid waste torrefied pellets [21] and briquettes [15]. These studies collectively provide valuable insights into the reactivity, flammability, and thermal properties of these biomass materials, exhibiting their potential as fuels and their role in sustainable energy solutions.

The T_i is the lowest temperature at which solid fuel initiates ignition in air without requiring an external ignition source [2]. Ignition of biomass is a pivotal stage that initiates combustion. A lower D_i indicates that the biomass can be easily ignited and combusted at lower temperatures, while a higher D_i indicates that the biomass requires higher temperature to ignite and combust [22], making it more challenging to start the combustion process. Biomass with a higher volatile matter poses a lower T_i and lower D_i, exhibiting ease of combustion [23]. It is important for biomass to ignite neither too quickly nor too slowly. Therefore, calculating the D_i is essential for understanding biomass ignition properties. The T_f indicates the temperature at which the combustion process of the biomass is completed [19]. A high D_f signifies complete combustion, leaving minimal unburned fuel or ash content [19,22]. A higher D_i and D_f indicate greater reactivity of the biomass, making it more suitable and flammable as a fuel [21]. The peak temperature is the point on the TGA curve at which the rate of weight loss of biomass due to combustion is at its maximum. This value typically varies around 280–300 °C [8]. For a thorough assessment of combustion behavior, it is essential to consider the S_i, which integrates three main properties of biomass combustion: ignition, burnout, and combustion characteristics [12]. A higher value of the S_i indicates efficient combustion, characterized by early ignition and thorough burnout [12,24,25]. Similarly, C_i is a crucial factor in assessing the fire risk and combustion behavior of biomass fuels. A higher C_i will have better combustion stability. It indicates that biomass can ignite easily at lower temperatures, releasing excess heat during combustion and supporting strong flames [26]. All of these indices provide valuable insights into the combustion characteristics of various biomass samples, enabling informed decisions when selecting suitable biomass and optimizing combustion system designs for efficient energy production and the effective use of the biomass as a fuel source, all while carefully considering safety aspects.

NIRS is one of the non-destructive, rapid, and low operation cost methods that do not require the employment of chemicals and chemical expertise. A mathematical correlation is established between the spectral and reference data of samples, containing either full wavelength ranges or a few significant wavelengths. This correlation is used to create the calibration equation for the prediction and evaluation of properties of biomass [27], such as elemental compositions (C, H, N, and S), determined by ultimate analysis [28,29], as well as moisture, volatile matter, fixed carbon, and ash content, assessed by proximate analysis [29,30]. The approach demonstrates acceptable performance and serves as an alternative to reference analysis, i.e., ultimate analysis and proximate analysis, which are characterized by their destructive nature, complexity, time-consuming process, and high operational costs, requiring chemicals and chemical expertise. The proximate constituents affect combustion performance [31], as well as the elemental composition, e.g., ignition temperature, which is determined by the H/C ratio and some other parameters [32], indicating the possibility of using NIRS to determine the combustion performance of biomass or fuel.

To the best of our knowledge, no study has been conducted to non-destructively evaluate combustion performance indices, such as the D_i, D_f, C_i, and S_i in chipped and ground biomass using FT-NIRS. Therefore, this research is structured into two main sections.

The first section involves determining the combustion parameters, including t_i and T_i, t_f and T_f, the maximum combustion rate $\left(\frac{dw}{dt}_{max}\right)$, and the average combustion rate $\left(\frac{dw}{dt}_{mean}\right)$, using TGA to calculate the D_i, D_f, S_i, and C_i of biomass from fast-growing trees and agricultural residues. The second section focuses on developing calibration models using Full-PLSR, GA-PLSR, SPA-PLSR, the MP 5 range-PLSR, and the MP 3 range-PLSR for the non-destructive assessment of the D_i, D_f, S_i, and C_i in both chipped and ground biomass. Then, the best-performing PLSR-based model for each index is selected, establishing it as a rapid, reliable, non-destructive alternative method for assessing combustion performance indexes in both chipped and ground biomass.

The research outcomes will assist industries in selecting the most suitable biomass for cost-effective energy production and resource optimization. Additionally, the developed non-destructive evaluation methods will serve as an alternative method to other destructive thermal analysis methods. Furthermore, they will provide a foundation for designing safe, economical, and environmentally balanced biomass combustion systems.

2. Materials and Methods

Figure 1 illustrates the comprehensive research methodology employed to ascertain combustion performance indices and develop their predictive model utilizing TGA and NIRS.

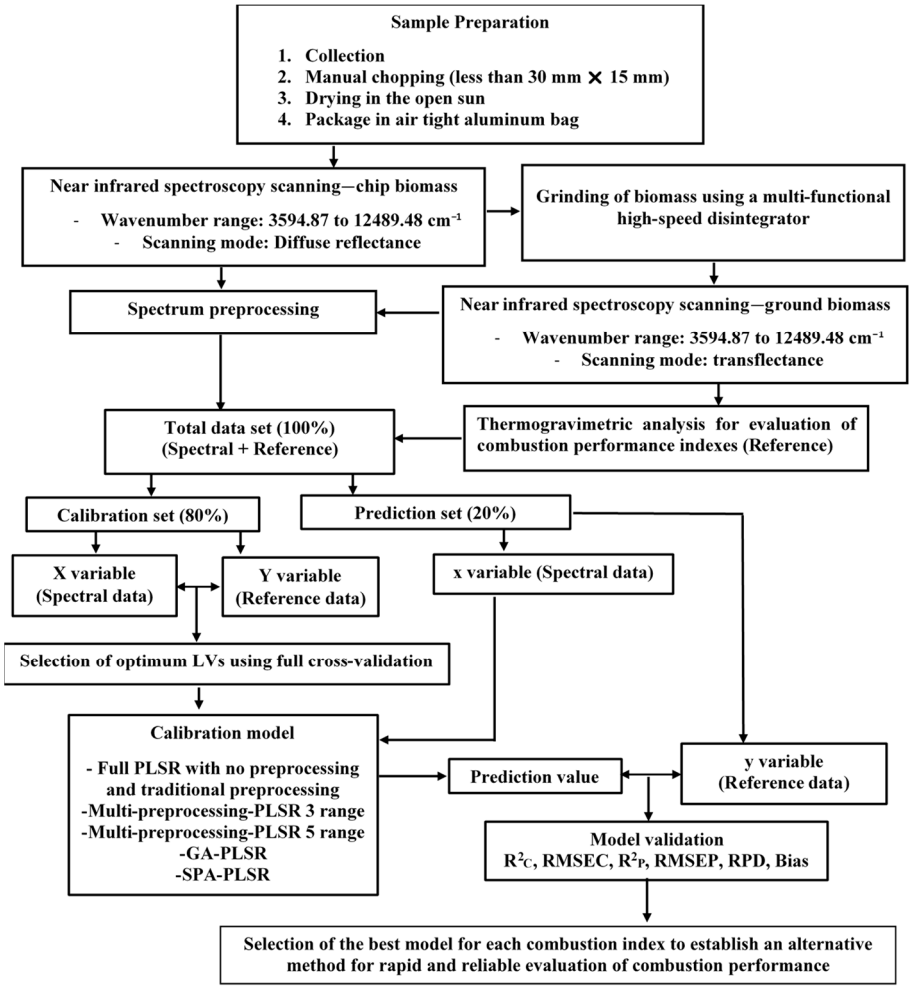

Figure 1. Flowchart illustrating the comprehensive research methodology for evaluating combustion performance indices of fast-growing trees and agricultural residues, using TGA in conjunction with NIRS combined with PLSR.

2.1. Sample Preparation

A total of ten different varieties of biomass samples were collected from the terai and mid-hill regions of Nepal, ranging from 86 to 1940 m above sea level, as representative samples. These biomass varieties are locally available and are commonly used in households and the industrial sector to fulfill their energy requirements. The biomass samples include fast-growing trees, i.e., *Alnus nepalensis* (11), *Pinux roxiburghii* (14), *Bombusa vulagris* (13), *Bombax ceiba* (11), and *Eucalyptus camaldulensis* (12), as well as agricultural residues, i.e., *Zea mays* (cob) (13), *Zea mays* (shell) (11), *Zea mays* (stover) (11), *Oryza sativa* (10), and *Saccharum officinarun* (9). A total of 115 samples were collected for this experiment. The samples were manually chopped, sun-dried until the weight of the samples reached equilibrium, and then approximately 350 gm of each sample were sealed in airtight aluminum bags to prevent air and moisture exchange [33]. They were transported to the Near-Infrared Spectroscopy Research Center for Agricultural Products and Food at the Department of Agricultural Engineering, School of Engineering, King Mongkut's Institute of Technology, Ladkrabang, Thailand, for FT-NIRS sample scanning and TGA experiments.

Initially, all the biomass samples were scanned in chip form using FT-NIRS. Afterward, the samples were ground using a multi-functional high-speed disintegrator (EF-04, Thai grinder, Thailand) and sealed in plastic zip-lock bags to allow the samples to have equilibrium moisture content with the laboratory surroundings and to prevent any contamination. In this study, three ground biomass samples were randomly selected and their particle size distribution was analyzed at Chulalongkorn University's Scientific and Technological Research Equipment Center in Bangkok, Thailand. This assessment was conducted using the Mastersizer 3000 instrument (MAL1099267, Hydro MV, Malvern, UK). The average particle size distribution of the ground biomass ranges between 0.01 and 3080 μm. All the ground samples were subsequently scanned again using the same FT-NIRS instrument to record the absorbance value at each wavenumber. The ground samples, which were sealed in plastic bags, were opened only during the TGA experiments.

2.2. FT-NIRS Scanning

All the biomass samples were scanned non-destructively using FT-NIRS (MPA, Bruker, Ettlingen, Germany) within the wavenumber range of 3594.87 to 12,489.48 cm^{-1}. Biomass chips were scanned using diffuse reflectance and sphere macro sample rotating mode, whereas ground biomass was scanned in the transflectance mode, both at a resolution of 16 cm^{-1}. Background and sample scans were set at 32 scans (average), with absorbance data logged as log(1/R), where R stands for reflectance. Both the chipped and ground biomass were scanned twice in a controlled, air-conditioned laboratory environment, with the temperature maintained at 25 ± 2 °C, without altering their positions. To obtain accurate and informative results without interference from background spectral data in the biomass samples, a gold plate scan was performed for every new sample, and aluminum plates and handles were used to prevent the leakage of near-infrared radiation.

2.3. Thermogravimetric Analysis Experiment

TGA is a destructive yet an effective method for studying the thermal behavior of biomass and for evaluating the combustion performance indices [3]. The TGA investigation is based on the mass loss of biomass samples during the entire experimental duration [21]. The combustion setting in TGA (TG 209 F3 Tarsus, Netzsch, Germany), with a microbalance sensitivity of 0.1 μg resolution, is programmed to simulate biomass direct combustion in air, i.e., with oxygen (99.7%) and nitrogen (99.99%) in a 1:4 ratio. The TGA experiment utilized ground biomass samples collected from the bottom of the glass vial that were used during NIRS scanning. These samples had an approximate average mass ranging from 6 to 29 mg, or one-third of the crucible volume, and were used for direct combustion. The biomass samples were combusted in a 6.8 mm diameter aluminum oxide (Al_2O_3) crucible within a temperature range of 35 °C to 700 °C, with a heat flow rate of 10 °C/min. Initially, the samples were isothermally held at 35 °C for 10 min. Nitrogen (99.99%) was utilized as a

protective layer in TGA to create a stable and inert environment, shielding the sample and preventing unwanted reactions with the surrounding air during thermal analysis, ensuring accurate analysis [34]. The thermal behavior of the biomass samples was analyzed by TG and DTG curves. Al_2O_3 crucibles were cleaned thoroughly using distilled water, followed by oven drying for 24 h to remove moisture content. The TGA instrument was calibrated regularly with an empty, clean Al_2O_3 crucible.

2.4. Reference Data Calculation

The TG and DTG profiles were analyzed using Proteus 6.0.0 (NETZSCH software, Germany) to determine the key combustion parameters, including the maximum combustion rate $\left(\frac{dw}{dt}_{max}\right)$, its corresponding time (t_p), and temperature (T_{max}) at which the maximum combustion rate occurs. The analysis also involved calculating the average combustion rate $\left(\frac{dw}{dt}_{mean}\right)$, t_i, T_i, t_f, T_f, and $\Delta t_{1/2}$, representing the time range at which the combustion rate is half of the $\left(\frac{dw}{dt}_{max}\right)$ value, measured in minutes. These parameters were used to compute combustion performance indices, such as D_i, D_f, S_i, and C_i, considering only one maximum mass loss peak, which collectively characterize the properties and performance of biomass combustion. The above-mentioned combustion performance indexes were calculated as follows [11]:

$$D_i = \frac{\frac{dw}{dt}_{max}}{t_p t_i} \quad (1)$$

$$D_f = \frac{\frac{dw}{dt}_{max}}{\Delta t_{1/2} t_p t_f} \quad (2)$$

$$S_i = \frac{\frac{dw}{dt}_{max} \times \frac{dw}{dt}_{mean}}{T_i^2 T_f} \quad (3)$$

$$C_i = \frac{\frac{dw}{dt}_{max}}{T_i^2} \quad (4)$$

2.5. Outlier Identification

Identification and removal of outliers from the total dataset is a critical step before developing any calibration model. In this study, outliers for reference data are identified using the following equation [35]:

$$\frac{(X_i - \overline{X})}{SD} \geq |\pm 3| \quad (5)$$

where X_i is the measured value of sample i, and $\overline{X}$ and SD denote the average and standard deviation of the measured values across all samples. If the outlier equation is satisfied, the sample is considered an outlier and is subsequently removed from the total data set.

In addition, if performance of the model was not satisfactory, outliers were further identified using the reference and NIR absorbance data. To achieve this, a comprehensive full cross-validation was conducted to obtain the prediction values for each biomass sample. A scatter plot was then created, comparing the measured and predicted values of the calibration set. The rigorous outliers were carefully identified and subsequently removed if their patterns notably diverged from the majority of data points to improve model accuracy.

2.6. Partial Least Squares Regression Modeling

After the NIRS scanning (optical data) and the calculation of combustion performance indices (reference data) based on TG and DTG curves obtained through TGA, PLSR-based regression models were developed. Five different types of PLSR-based models were employed, namely Full-PLSR, multi-preprocessing PLSR-5 range, multi-preprocessing

PLSR-3 range, GA-PLSR, and SPA-PLSR (refer to Figure 1). In this study, after running the data in ascending order, the total data set was manually divided into an 80% calibration set and a 20% validation set, where the first 8 samples were assigned to the calibration set and the following 2 were assigned to the validation set. The process was repeated until every sample was assigned. Both maximum and minimum reference data must be included in the calibration set, ensuring coverage across a wide range [33,35].

Full-PLSR includes the traditional approach of employing various spectral preprocessing techniques to develop a PLSR model. These techniques include raw spectra, constant offset, SNV, MSC, D1, D2, vector normalization, min-max normalization, mean centering, D1 + vector normalization, and D1 + MSC. In the multi-preprocessing 5-range method and the multi-preprocessing 3-range method, the entire available wavenumber range is divided into five and three distinct sections, respectively. Entire divided sections undergo pre-treatment using a series of the most effective combinations of various preprocessing techniques within the range of 3595 to 12,489 cm^{-1}. Under the multi-preprocessing techniques, seven different types of preprocessing techniques have been employed and labeled as follows: (0) Zero, indicating a zero absorbance value for all the wavenumbers in the particular section, (1) raw spectra, (2) SNV, (3) MSC, (4) D1, (5) D2, and (6) constant offset. All possible preprocessing combination sets are created, and a full cross-validation is performed using PLSR on the total data set to identify the best preprocessing combination set. PLSR models are then developed based on this optimal combination set [33]. GA-PLSR and SPA-PLSR are optimization techniques that select the most influential wavenumbers for the development of a PLSR model [36]. The NIRS total dataset in this study contains 1154 dependent variables, which can potentially lead to issues of multicollinearity and overfitting during modeling. By efficiently identifying the most relevant wavenumbers, these optimization techniques address these challenges, resulting in a more accurate and efficient predictive model. After the models were optimized, they were externally validated using a validation set comprising 20% of the total samples collected. The validation was done by subjecting the validation sample spectra to the models and comparing the true (measured) values of the samples to the predicted values.

The performance of the models was compared based on the following statistical parameters: R^2_C and R^2_P, RMSEC and RMSEP, RPD and bias.

In this study, the interpretation of the coefficient of determination was performed based on Williams et al.'s (2019) guidelines [37], and the RPD value was assessed using the guideline proposed by Zornoza et al. (2008) [38]. The selection of the best model was based on higher values for R^2_C, R^2_P, and RPD, as well as lower RMSEC and RMSEP values. However, in the case of similar performance, the model with a lower number of LV_s was selected as the best-performing model. For the overall modeling, a built-in code from MATLAB-R2020b (MathWorks, Natick, MA, USA) was utilized.

3. Results and Discussion

3.1. NIR Spectra of Fast-Growing Trees and Agricultural Residues

Figure 2 shows the average raw spectra of fast-growing trees and agricultural residues from (a) chip biomass obtained through the diffuse reflectance mode of FT-NIRS scanning and (b) ground biomass obtained through the transflectance mode of FT-NIRS scanning, covering the full wavenumber range from 3595 to 12,489 cm^{-1}, under a controlled air-conditioned laboratory environment. The temperature was maintained at 25 ± 2 °C and the moisture content inside the spectrometer was absorbed by molecular sieve pellets. A significant variation is notable in the raw spectra between the chip and ground biomass samples. The ground biomass exhibited lower signal intensities, sharper and better-defined absorption peaks, as well as a reduced presence of baseline variability. These distinct observations are attributed to the small particle size and homogeneous nature of the biomass sample.

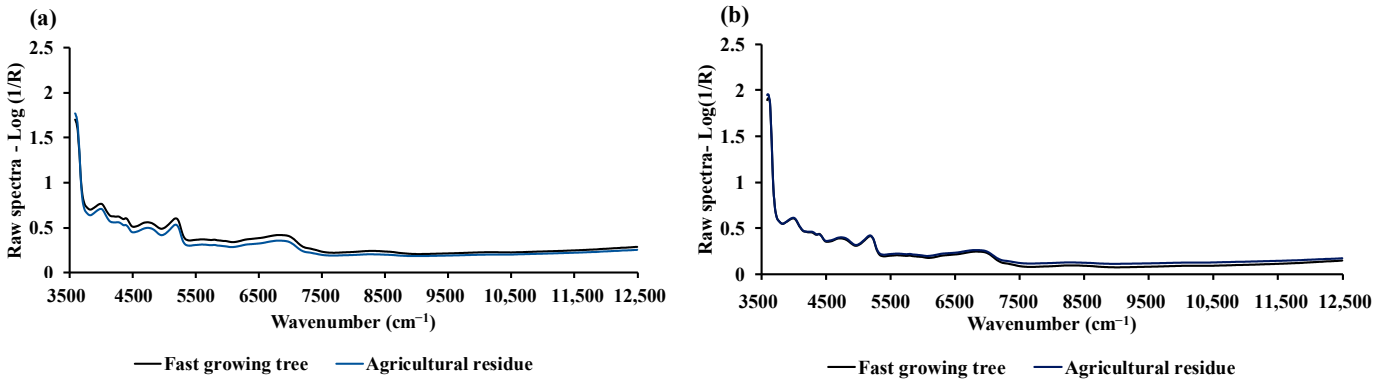

Figure 2. Average raw spectra of fast-growing trees and agricultural residue for (**a**) chip biomass obtained through diffuse reflectance mode and (**b**) ground biomass obtained through transflectance mode of FT-NIRS scanning.

3.2. Combustion Characteristic Parameters and Combustion Performance Indices from TGA

Figure 3 shows the typical TG and DTG curves of ten distinct biomass samples obtained via TGA, which has been utilized to calculate combustion performance indices and for PLSR modeling.

The selection of an appropriate biomass fuel is a crucial decision, heavily reliant on various essential parameters, such as energy production potential, the efficiency of the combustion process, required burning duration, compatibility with the system's specifications, environmental considerations, and availability [39,40]. Therefore, it is of utmost importance to understand the biomass combustion characteristic parameters at different times and temperatures, as well as the overall combustion performance indices, before designing and developing a combustion system to fulfill energy needs and demands. TG and DTG curves obtained via TGA are instrumental in investigating combustion characteristics parameters and their indices. The TG curve represents mass loss as a function of time or temperature, whereas the DTG curve represents the time derivative of the sample mass loss [20]. With a combined analysis of TG and DTG curves, a comprehensive evaluation of the combustion characteristic parameters and combustion performance indices can be achieved. T_i on the DTG curve is the point where the mass loss rate reaches 1%/min after the initial weight loss caused by the moisture. T_f marks the point at which the burning rate reaches 1%/min at the end of the DTG curve [41,42]. T_{max}, also known as peak temperature, is represented on the DTG curve where the biomass mass loss rate is the highest. Correspondingly, t_i, t_f, and t_p denote the recorded times for T_i, T_f, and T_{max}. $\Delta t_{1/2}$ is the time range at which the combustion rate is half of the $\left(\frac{dw}{dt}_{max}\right)$ value, and $\frac{dw}{dt}_{mean}$ is the average conversion rate between T_i and T_f [41].

The normal distribution of all the combustion performance reference data, including D_i, D_f, S_i, and C_i was analyzed using a one-sample Kolmogorov–Smirnov test in SPSS 16.0. The corresponding *p*-values for D_i, D_f, S_i, and C_i were calculated as 0.893, 0.033, 0.000, and 0.608, respectively.

Considering the significance level of 0.05, it is observed that the *p*-values for D_i and C_i are greater than 0.05. As a result, the reference data for D_i and C_i, utilized in the PLSR modeling study, are considered to exhibit a uniform distribution. In contrast, the obtained *p*-values for D_f and S_i are less than 0.05, indicating a departure from a uniform distribution for these variables. Therefore, as explained in Section 2.5, the identification and removal of outliers from the total dataset of D_f and S_i become imperative. This step is crucial for enhancing the validity and reliability of the model developed in this research, as outliers can significantly impact the accuracy and robustness of the findings.

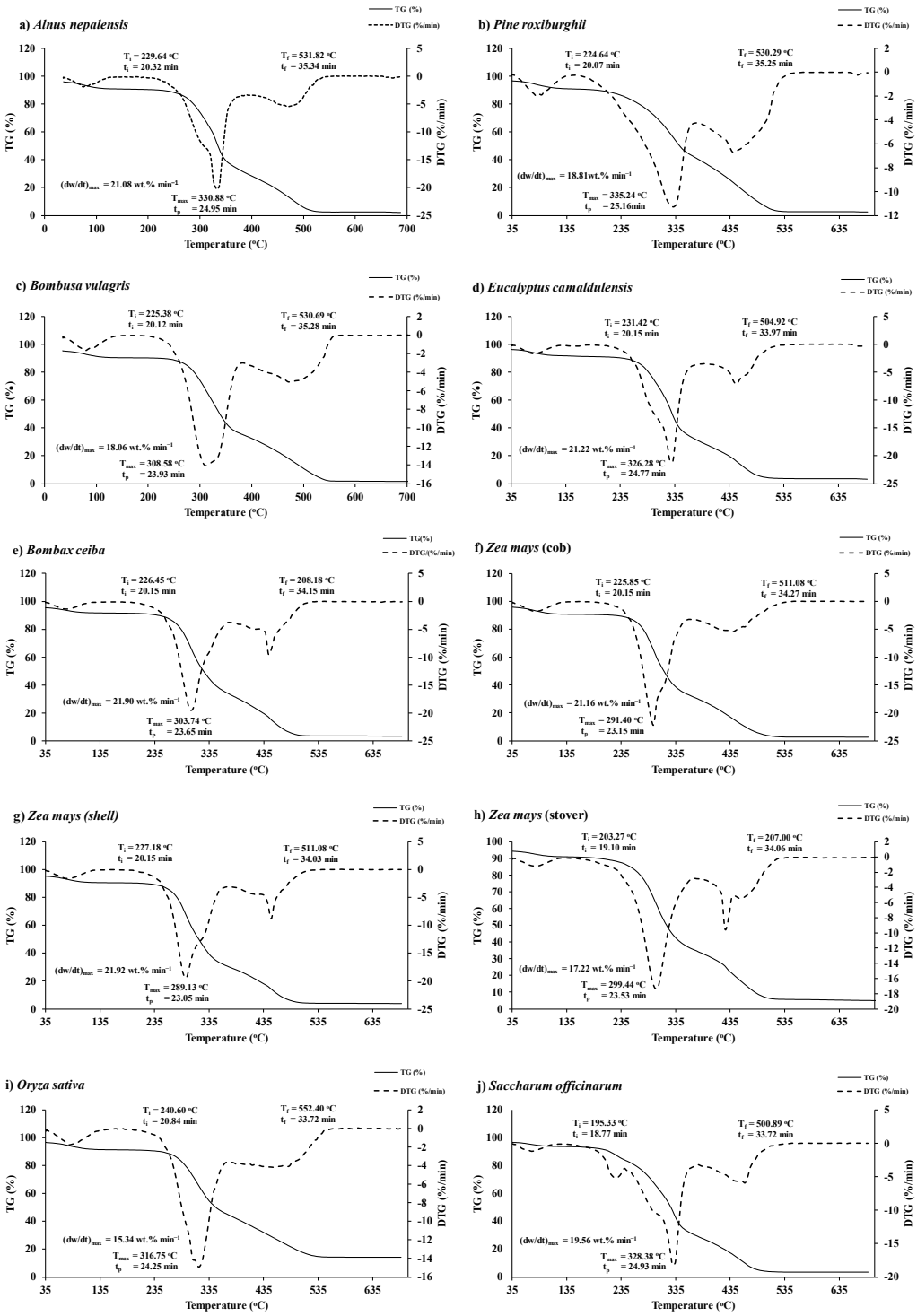

Figure 3. TG and DTG curves obtained via TGA within the temperature range of 35 to 700 °C for (**a**) Alnus nepalensis, (**b**) Pinus roxiburghii, (**c**) Bombusa vulagris, (**d**) Eucalyptus camaldulensis, (**e**) Bombax ceiba, (**f**) Zea mays (cob), (**g**) Zea mays (shell), (**h**) Zea mays (stover), (**i**) Oryza sativa, and (**j**) Saccharum officinarum.

Table 1 summarizes the average combustion characteristic parameters (t_p, T_{max}, t_i, T_i, t_f, T_f, $\frac{dw}{dt}_{max}$, $\frac{dw}{dt}_{mean}$, $\Delta t_{1/2}$) and combustion performance indices (D_i, D_f, S_i, C_i) of the fast-growing trees and agricultural residues obtained through the combined analysis of TG and TGA curves (refer to Figure 3). During direct combustion, the first stage involves the removal of moisture from the biomass, a process represented by the gradual thermal

degradation of the biomass. This typically takes place within a temperature range of 35–140 °C. The second stage involves devolatilization and its combustion, which occurs at temperatures around 150–405 °C and is characterized by a rapid loss of mass. The third stage involves the char combustion, during which the rate of mass loss decreases and gradually slows down until the sample eventually turns into ash [21].

From Table 1, it is evident that fast-growing trees and agricultural residues are slightly different in both active combustion temperature ranges and time ranges. For fast-growing trees, the average active combustion temperature range was 227.51–521.18 °C, with a corresponding average time range of 20.22–34.80 min. For agricultural residues, the average active combustion temperature range was 218.45–515.51 °C, and the average time range was 19.8–34.49 min. The average maximum combustion rates recorded were 20.21 wt.% min^{-1} at 320.94 °C for fast-growing trees and 19.04 wt.% min^{-1} at 305.02 °C for agricultural residues.

The values of T_i and T_f for fast-growing trees ranged from 224.64 to 231.42 °C and from 504.92 to 531.82 °C, respectively. Similarly, for agricultural residues, the values ranged from 195.33 to 240.60 °C and from 500.89 to 552.40 °C. The higher values of T_i and T_f in fast-growing trees signify that fast-growing trees are more difficult to ignite, but they combust for a longer period and turn into ash more slowly than agricultural residues. The presence of high lignin content and low volatile matter in fast-growing trees may contributes to the elevated T_i and T_f [42,43]. The D_i of both fast-growing trees and agricultural residue is similar, while the D_f of fast-growing trees is comparatively higher than that of agricultural residues. The S_i, which assesses both the ignition and burnout characteristics of the fuel, indicating the efficiency of combustion conversion, is high for agricultural residues. This demonstrates that agricultural residues are easier to burn, indicating their higher thermal and combustion reactivity as a fuel source. Additionally, the higher C_i of agricultural residues indicates its better combustion stability.

3.3. Modeling for Combustion Performance Indices

Table 2 presents statistical data on the combustion performance indices: D_i, D_f, S_i, and C_i. These indices were employed in the development of the PLSR-based model for both chipped and ground biomass. Prior to model development, outliers were identified and were subsequently removed from the total dataset (refer to Section 2.5). The entire dataset was then partitioned, with 80% of the data being allocated to the calibration set containing the highest and lowest combustion performance index values, and 20% to the prediction set for both chipped and ground biomass. As elaborated in Section 2.6, five distinct PLSR-based regression models were formulated for each index: the full-PLSR model, the multi-preprocessing PLSR-5 range model, the multi-preprocessing PLSR-3 range model, the GA-PLSR model, and the SPA-PLSR model. These models incorporated various preprocessing techniques. The performance of each model was compared, and the best model for each technique is listed. Tables 3 and 4 display the overall performance of the PLSR-based model for each index in chipped and ground biomass, respectively. The model with the best performance is indicated in bold. Figure 4 shows the average spectrum preprocessing for each combustion performance indices obtained for chip and ground biomass from the best performance model.

3.3.1. Ignition Index (D_i)

From the data in Tables 3 and 4, by R^2_P determination, the performance of D_i using the multi-preprocessing PLSR-5 range method for ground biomass has improved by 4.5645% compared to that of the traditional approach, i.e., the full-PLSR method.

Figure 5a,e show the scatter plots of the measured and predicted D_i values from the calibration and prediction sets for chip and ground biomass, respectively, using the full-PLSR and the multi-preprocessing PLSR-5 range methods.

Table 1. Combustion parameters and performance indices for fast-growing trees and agricultural residue subjected to direct combustion using TGA.

Category	Biomass Sample	Combustion Parameters									Combustion Performance Indices			
		$(dw/dt)_{max}$	$(dw/dt)_{mean}$	T_i	T_f	T_{max}	t_i	t_f	t_p	$\Delta t_{1/2}$	D_i (10^{-2})	D_f (10^{-3})	S_i (10^{-6})	C_i (10^{-4})
		(wt.% min^{-1})	(wt.% min^{-1})	(°C)	(°C)	(°C)	(min)	(min)	(min)	(min)	wt.%.min^{-3}	wt.%.min^{-4}	wt.%^{2}.min^{-2}.C^{-3}	wt.%min^{-1}.$°C^{-2}$
Fast-growing trees	*Alnus nepalensis*	21.08	2.83	229.64	531.82	330.88	20.32	35.34	24.95	5.19	4.15	4.79	2.54	3.99
	Pinus roxiburghii	18.81	2.85	224.64	530.29	335.24	20.07	35.25	25.16	5.04	3.71	4.43	2.71	3.71
	Bombusa vulagris	18.06	2.67	225.38	530.69	308.58	20.12	35.28	23.93	5.68	3.76	4.60	2.41	3.60
	Eucalyptus camaldulensis	21.22	2.77	231.42	504.92	326.28	20.43	33.97	24.77	4.60	4.20	5.09	2.54	3.96
	Bombax ceiba	21.90	2.65	226.45	508.18	303.74	20.15	34.15	23.65	5.25	4.61	6.05	2.41	4.30
Agricultural residues	*Zea mays* (cob)	21.16	2.80	225.85	511.08	291.40	20.15	34.27	23.15	5.56	4.54	6.18	2.49	4.15
	Zea mays (shell)	21.92	2.78	227.18	506.18	289.13	20.19	34.03	23.05	28.54	4.71	1.25	2.46	4.25
	Zea mays (stover)	17.22	2.48	203.27	507.00	299.44	19.10	34.06	23.53	5.27	3.84	4.26	2.87	4.30
	Oryza sativa	15.34	2.49	240.60	552.40	316.75	20.84	36.37	24.25	6.06	3.04	3.88	1.89	2.65
	Saccharum officinarum	19.56	2.82	195.33	500.89	328.38	18.77	33.72	24.93	4.39	4.18	4.31	3.75	5.20

Table 2. Statistical data of combustion performance parameters for ground and chipped biomass of fast-growing trees and agricultural residue used in model development (after outliers were removed from the total of 115 samples).

Biomass	Parameter (Ground)	Units	N_T	Calibration Set					Validation Set				
				Nc	Max	Min	Mean	SD	Np	Max	Min	Mean	SD
Ground	Ignition index D_i (10^{-2})	wt.%.min^{-3}	103	82	5.3496	2.4171	4.0699	0.6510	21	5.0998	2.8155	3.8740	0.7008
	Burnout index D_f (10^{-3})	wt.%.min^{-4}	87	70	6.7591	1.0380	4.2231	1.3066	17	6.5259	1.2071	4.2180	1.2905
	Comprehensive combustion index S_i (10^{-6})	wt.%^{2}.min^{-2}.$°C^{-3}$	107	86	4.0363	1.6140	2.5704	0.4551	21	4.0296	1.7917	2.5502	0.4649
	Flammability index C_i (10^{-4})	wt.%.min^{-1}.$°C^{-2}$	114	91	6.5187	2.3349	3.9879	0.8590	23	5.3362	2.4757	3.8578	0.6980
Chip	Ignition index D_i (10^{-2})	wt.%.min^{-3}	102	82	5.3500	2.7000	4.0532	0.6295	20	5.1000	2.8200	3.8975	0.7098
	Burnout index D_f (10^{-3})	wt.%.min^{-4}	94	75	7.1715	1.0380	4.4178	1.3070	19	6.9777	1.1030	4.5240	1.4880
	Comprehensive combustion index S_i (10^{-6})	wt.%^{2}.min^{-2}.$°C^{-3}$	102	82	4.0363	1.7584	2.5577	0.4478	20	4.0296	1.7917	2.5325	0.4697
	Flammability index C_i (10^{-4})	wt.%.min^{-1}.$°C^{-2}$	112	90	6.2216	2.3349	3.9384	0.7779	22	5.3362	2.4757	3.8255	0.6966

Table 3. Results of the PLSR-based model for the combustion performance indices of chip biomass, with the model showing the best performance highlighted in bold.

Parameter (Chip)	Units	Algorithm	Preprocessing	LVs	Calibration Set		Validation Set			
					R^2_C	RMSEC	R^2_P	RMSEP	RPD	Bias
D_i	wt.%.min^{-3}	**Full-PLSR**	**Second derivative**	**6**	**0.6491**	**0.3706**	**0.6100**	**0.4321**	**1.6**	**−0.0996**
		SPA-PLSR	Vector normalization (SW: 130)	9	0.6101	0.3907	0.5994	0.4379	1.6	−0.0770
		GA-PLSR	Vector normalization (SW: 518)	8	0.6479	0.3713	0.6073	0.4335	1.6	−0.1094
		MP-PLSR: 5-Range	Combination set: 2,4,0,5,5	4	0.5962	0.3976	0.5929	0.4414	1.6	−0.1071
		MP-PLSR: 3-Range	Combination set: 2,5,4	4	0.6015	0.3950	0.6008	0.4371	1.6	−0.0764
D_f	wt.%.min^{-4}	Full-PLSR	Constant offset	9	0.7470	0.6531	0.6920	0.8045	1.9	0.2043
		SPA-PLSR	Constant offset (SW: 717)	8	0.7335	0.6704	0.6738	0.8279	1.8	0.2549
		GA-PLSR	**Min-max normalization (SW: 64)**	**10**	**0.7141**	**0.6943**	**0.7019**	**0.7914**	**1.9**	**0.1245**
		MP-PLSR: 5-Range	Combination set: 6,6,4,6,0	9	0.7420	0.6596	0.6361	0.8744	1.7	0.1619
		MP-PLSR: 3-Range	Combination set: 1,6,6	10	0.7533	0.6450	0.6550	0.8515	1.8	0.2290
S_i	wt.%^{2}.min^{-2}.°C^{-3}	Full-PLSR	Raw spectra	9	0.7700	0.2136	0.7699	0.2196	2.1	0.0372
		SPA-PLSR	First derivative+MSC (SW: 346)	12	0.8153	0.1914	0.7484	0.2296	2.0	−0.0122
		GA-PLSR	**First derivative (SW: 18)**	**11**	**0.8006**	**0.1989**	**0.7812**	**0.2141**	**2.2**	**0.0535**
		MP-PLSR: 5-Range	Combination set: 3,5,3,6,0	9	0.8068	0.1958	0.7721	0.2185	2.2	0.0533
		MP-PLSR: 3-Range	Combination set: 6,2,4	3	0.6047	0.2800	0.5126	0.3196	1.4	−0.0414
C_i	wt.%min^{-1}.°C^{-2}	Full-PLSR	SNV	14	0.8215	0.3267	0.6119	0.4240	1.6	0.0523
		SPA-PLSR	Second derivative (SW: 213)	11	0.6797	0.4377	0.6439	0.4061	1.7	−0.0297
		GA-PLSR	Mean centering (SW: 16)	13	0.5744	0.5045	0.5666	0.4481	1.5	0.0823
		MP-PLSR: 5-Range	Combination set: 2,2,1,6,5	9	0.6469	0.4595	0.6853	0.3818	1.8	−0.0652
		MP-PLSR: 3-Range	**Combination set: 2,5,0**	**14**	**0.6903**	**0.4304**	**0.6766**	**0.3871**	**1.8**	**−0.0343**

Refer to the unit column for the RMSEC, RMSEP, and bias units for D_i, D_f, S_i, and C_i.

Table 4. Results of the PLSR-based model for the combustion performance indices of ground biomass, with the model showing the best performance highlighted in bold.

Parameter (Ground)	Units	Algorithm	Preprocessing	LVs	Calibration Set		Validation Set			
					R^2_C	RMSEC	R^2_P	RMSEP	RPD	Bias
D_i	wt.%.min^{-3}	Full-PLSR	Raw spectra	8	0.6533	0.3810	0.6466	0.4064	1.7	−0.0898
		SPA-PLSR	Raw (SW: 1132)	8	0.6542	0.3805	0.6472	0.4062	1.7	−0.0898
		GA-PLSR	Mean centering (SW:523)	9	0.6442	0.3859	0.6071	0.4286	1.6	−0.0743
		MP-PLSR: 5-Range	**Combination set: 3,5,3,1,0**	**9**	**0.7039**	**0.3521**	**0.6782**	**0.3879**	**1.8**	**−0.0016**
		MP-PLSR: 3-Range	Combination set: 1,4,6	13	0.7773	0.3053	0.5634	0.4518	1.5	−0.0511
D_f	wt.%.min^{-4}	Full-PLSR	First derivative (g = 5, s = 5)	11	0.8449	0.5111	0.8217	0.5286	2.4	0.0678
		SPA-PLSR	Second derivative(SW: 954)	10	0.8139	0.5598	0.8001	0.5598	2.2	0.0206
		GA-PLSR	**First derivative (SW:921)**	**11**	**0.8417**	**0.5163**	**0.8426**	**0.4968**	**2.5**	**0.0631**
		MP-PLSR: 5-Range	Combination set: 1,5,4,3,6	12	0.8151	0.5580	0.8018	0.5574	2.3	0.1177
		MP-PLSR: 3-Range	Combination set: 2,2,1	14	0.8240	0.5443	0.8137	0.5405	2.6	0.2432
S_i	wt.%^{2}.min^{-2}.°C^{-3}	**Full-PLSR**	**MSC**	**14**	**0.9028**	**0.1411**	**0.8808**	**0.1566**	**3.1**	**0.0532**
		SPA-PLSR	MSC (SW: 626)	13	0.8849	0.1536	0.8045	0.2005	3.0	0.1298
		GA-PLSR	MSC (SW: 60)	10	0.8567	0.1713	0.8566	0.1717	2.8	−0.0632
		MP-PLSR: 5-Range	Combination set: 4,4,5,6,4	12	0.9449	0.1062	0.8136	0.1958	2.3	0.0102
		MP-PLSR: 3-Range	Combination set: 4,2,1	13	0.9071	0.1380	0.8316	0.1861	2.5	−0.0257
C_i	wt.%min^{-1}.°C^{-2}	Full-PLSR	MSC	15	0.7881	0.3932	0.6914	0.3792	1.9	−0.1361
		SPA-PLSR	Raw (SW: 13)	15	0.7234	0.4492	0.6524	0.4025	1.8	−0.1162
		GA-PLSR	Raw (SW: 333)	9	0.5822	0.5520	0.5476	0.4592	1.5	−0.0477
		MP-PLSR: 5-Range	**Combination set: 3,2,1,1,4**	**12**	**0.7576**	**0.4205**	**0.7204**	**0.3610**	**2.0**	**−0.1310**
		MP-PLSR: 3-Range	Combination set: 1,2,4	15	0.7860	0.3951	0.6919	0.3790	1.9	−0.0884

Refer to the unit column for the RMSEC, RMSEP, and bias units for D_i, D_f, S_i, and C_i.

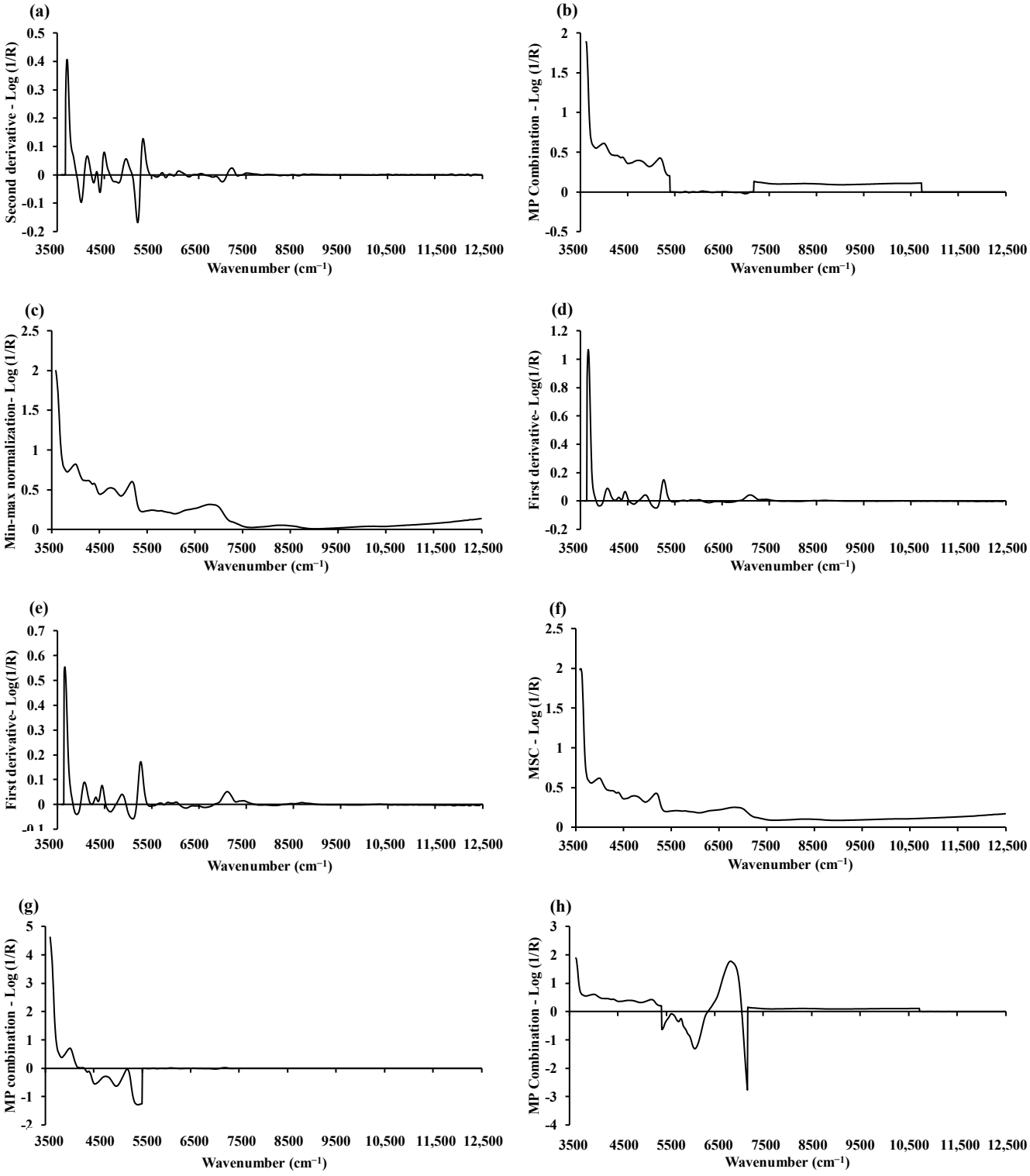

Figure 4. The average spectrum for (**a**) D_i in chip biomass is obtained by using the D2 (5,5). (**b**) D_i in ground biomass is obtained by using the multi-preprocessing PLSR-5 range with a combination set of 3,5,3,1,0. (**c**) D_f in chip biomass is achieved by using min-max normalization. (**d**) D_f in ground biomass is obtained by using D1 (5,5). (**e**) S_i in chip biomass is acquired by using D1 (5,5). (**f**) S_i in ground biomass is acquired by MSC. (**g**) C_i in chip biomass is calculated by using the multi-preprocessing PLSR-3 range method with a combination set of 2,5,0. (**h**) C_i in ground biomass is determined by the multi-preprocessing PLSR-5 range method with a combination set of 3,2,1,1,4.

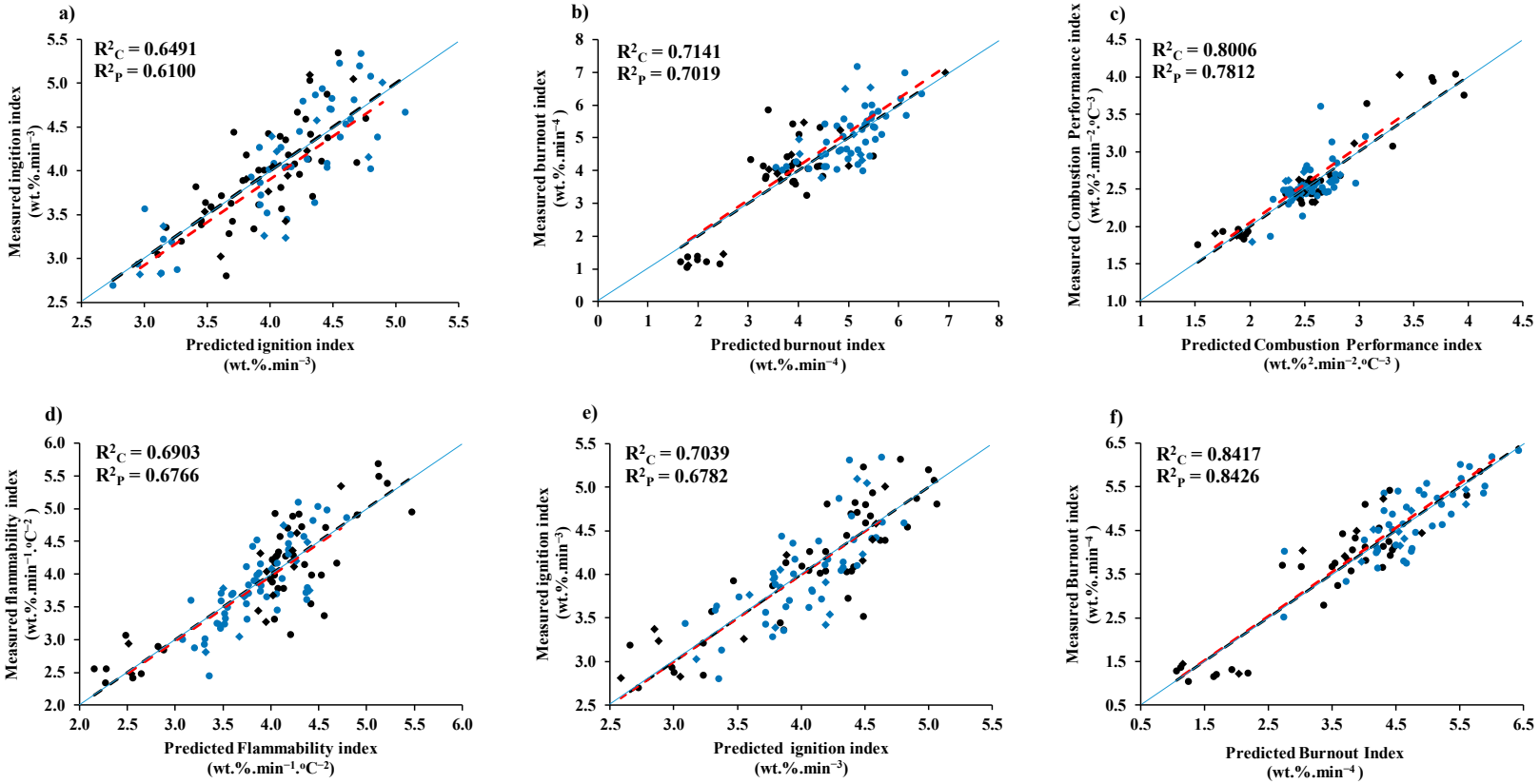

Figure 5. *Cont.*

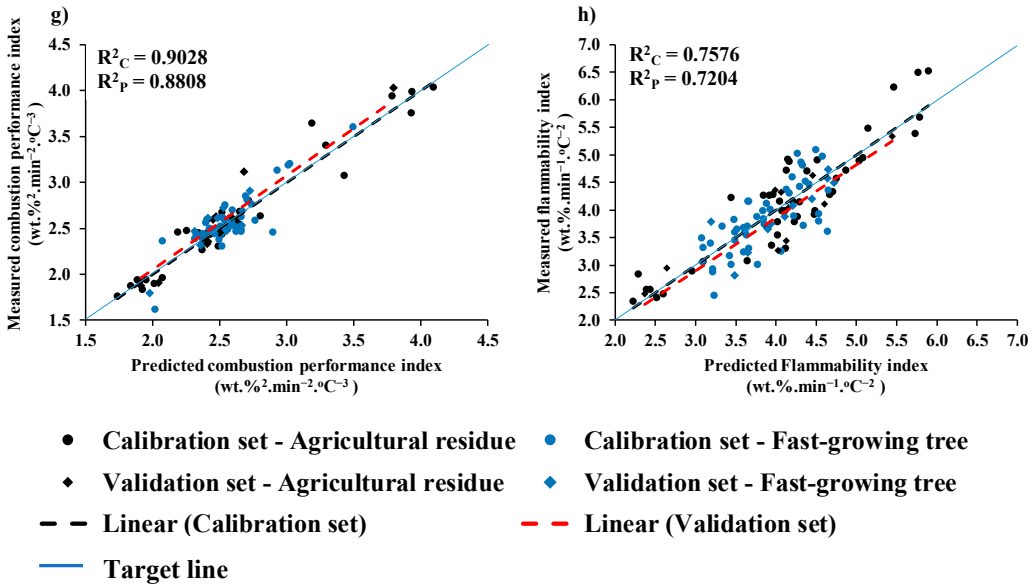

Figure 5. Measured versus predicted value in calibration set and validation set for chip biomass: (**a**) ignition index, (**b**) burnout index, (**c**) combustion performance index, and (**d**) flammability index; and for ground biomass: (**e**) ignition index, (**f**) burnout index, (**g**) combustion performance index, and (**h**) flammability index.

The regression coefficient plot from the full-PLSR D2 analysis for chip biomass is presented in Figure 6. The most important peaks are observed in the regression coefficient plot, specifically at wavenumbers 3722, 4405, 5200, 5787, 12,048, and 12,300 cm^{-1}. These peaks might have a significant influence on enhancing the performance of the model in evaluating the D_i in chip biomass.

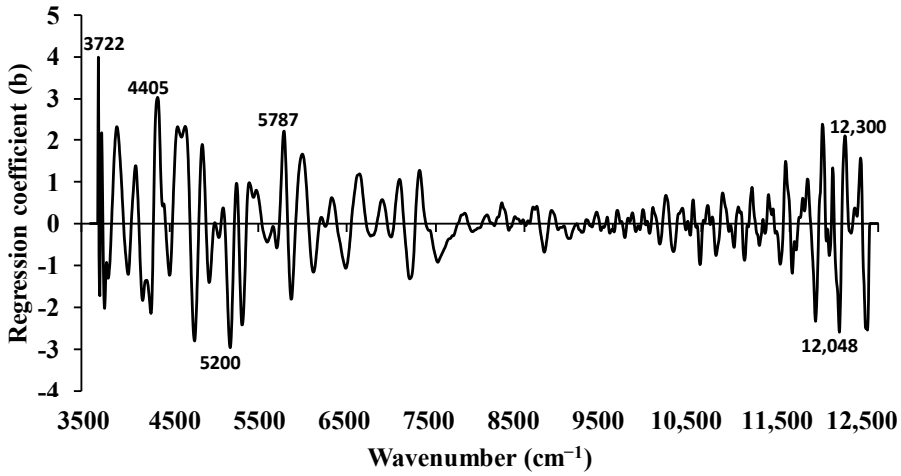

Figure 6. The regression coefficient for the D_i of chip biomass using the full-PLSR approach with spectral preprocessing of D2.

Similarly, Figure 7 displays the regression coefficient plot for the D_i of ground biomass, obtained using the multi-preprocessing PLSR-5 range method. The important peaks are noticed at wavenumbers 3650, 4608, 5495, and 8754 cm^{-1}, which might significantly influence the model's performance. Here, regression coefficient values within the range of 10,723–12,489 cm^{-1} are observed to be zero. This observation suggests that the variable in this section, which is assigned a zero absorbance using empty preprocessing, may not possess sufficient variation in the dataset to yield meaningful predictive power.

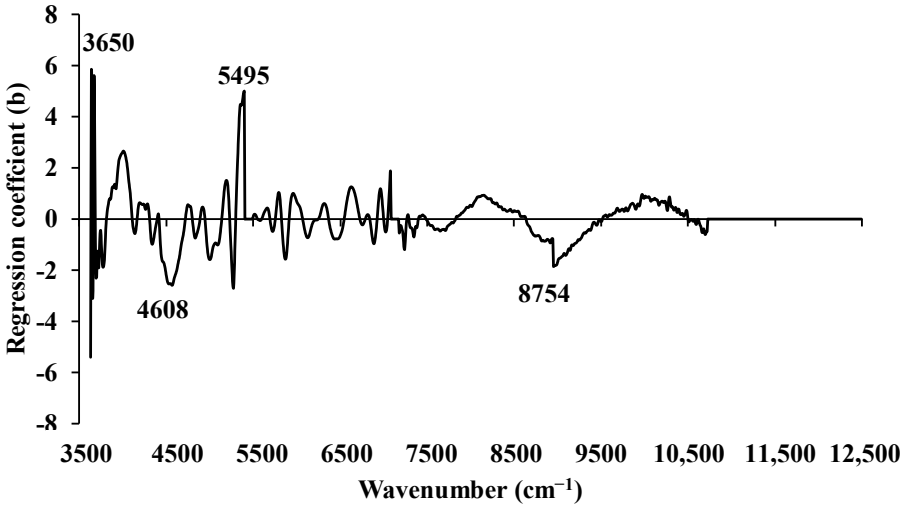

Figure 7. The regression coefficient for the D_i of ground biomass using the multi-preprocessing PLSR-5 range method with a spectral preprocessing combination set of 3, 5, 3, 1, 0.

Table 5 displays the functional groups, spectra-structure, and material types corresponding to the specific peak wavenumbers observed in the regression coefficient plots through NIRS analysis of chip and ground biomass for D_i [44].

Table 5. The dominant peaks on the regression coefficient plot and average absorbance plot obtained via the best-performing PLSR-based model [44].

Combustion Performance Index	Biomass Type	Peak Wavenumber (cm^{-1})	Functional Group	Spectra-Structure	Material Type
D_i	Chip	3722	C−H aromatic		C−H aryl
		4405		O−H stretching and C−O stretching	cellulose
		5200		O−H stretching and HOH deformation combination	O−H molecular water
		5787	C−H methylene ($.CH_2$) (asymmetric)		Hydrocarbons, aliphatic
		12,048	C−H methylene C−H		Hydrocarbons, aliphatic
		12,300		C−H combination	Hydrocarbons, aliphatic
	Ground	3650	O−H from primary alcohols as (-CH-OH)	O−H (ν)	Primary alcohols
		4608		C−H stretching and C−H deformation combination	Alkenes
		5495	O−H/C−H combination	O−H stretching and C−O stretching ($3\nu_s$) combination	Cellulose
		8754	C−H aromatic (ArCH)	C−H (3ν), aromatic C−H	Hydrocarbons, aromatic
D_f	Chip	4019		C−H stretching and C−C stretching combination	Cellulose
		5181		O−H stretching and HOH bending combination	Polysaccharides
		6319	O−H stretching band, alkyl alcohols or water		Alcohols or water O−H
		9960	O−H from secondary alcohols as (−CH−OH)	O−H (3ν)(−CH−OH)	Secondary alcohols
	Ground	3650	O−H from primary alcohols as (−CH−OH)	O−H (ν)	Primary alcohols
		4019		C−H stretching and C−C stretching combination	Cellulose
		5200		O−H stretching and HOH deformation combination	O−H molecular water
		6897		O−H (2ν)	Starch/polymeric alcohol
S_i	Chip	4019		C−H stretching and C−C stretching combination	Cellulose
		4292		C−H stretching and CH_2 deformation combination	Polysaccharides
		7092	O−H alcohol (RO−H)	O−H (2ν)	Hydrocarbons, aliphatic
	Ground	4525	N−H ammonia in water	N−H (3ν) for NH_3 in water	Ammonia in water
		4762		O−H bending and C−O stretching combination	Polysaccharides
		5376		C−Cl (7ν)	Chlorinated hydrocarbons
		5869		C−H (2ν), methyl C−H (symmetric)	Hydrocarbons, aliphatic
		7092	O−H alcohol (RO−H)	O−H (2ν)	Hydrocarbons, aliphatic
		12,300		C−H combination	Hydrocarbons, aliphatic
C_i	Chip	4202		C−H stretching and C−C stretching combination	Lipids
		4307		C−H stretching and CH_2 deformation combination	Polysaccharides
		5241	P−OH phosphate (.P-OH)	O−H (2ν)	Phosphate
		5495	O−H/C−H combination	O−H stretching and C−O stretching ($3\nu_s$) combination	Cellulose
	Ground	5495	O−H/C−H combination	O−H stretching and C−O stretching ($3\nu_s$) combination	Cellulose
		5900	C−H methyl ($.CH_3$)	C−H (2ν), $.CH_3$	Hydrocarbons, methyl
		6666	N−H combination band from urea ($NH_2-C=O-NH_2$)		N−H from urea
		6736	N−H band from urea ($NH_2-C=O-NH_2$)	N-H (2ν) symmetric stretching from urea	Urea

ν: Fundamental stretching vibration absorption band, 2ν: first overtone of fundamental stretching band, 3ν: second overtone of fundamental stretching band, 7ν: six overtone of fundamental stretching band.

3.3.2. Burnout Index (D_f)

As shown in Tables 3 and 4, the best-performing PLSR-based models for both chip and ground biomass were obtained using GA-PLSR. For chip biomass, GA selected 64 out of 1154 influential wavenumbers with spectral preprocessing using min-max normalization (refer to Figure 5c). For ground biomass, GA selected 921 out of 1154 wavenumbers with spectral preprocessing using the D1 (segment = 5, gap = 5) (refer to Figure 5d). Figure 5b,f show the scatter plots for measured versus predicted D_f for chip and ground biomass.

By R^2_P determination, the GA-PLSR model performance of D_f in chip biomass has improved by 1.6332% compared to the full-PLSR method.

Figure 8 shows the average absorbance spectrum pretreated with min-max normalization, using red marks to emphasize important wavenumbers identified through GA.

The selected significant wavenumbers, located at 4019, 5181, 6319, and 9960 cm^{-1}, could potentially exert a notable influence on the model's performance in evaluating the D_f in the chip biomass samples. Similarly, Table 5 presents the associated functional groups, spectra-structure, and the material type corresponding to specific peak wavenumbers observed in D_f chip biomass samples [44].

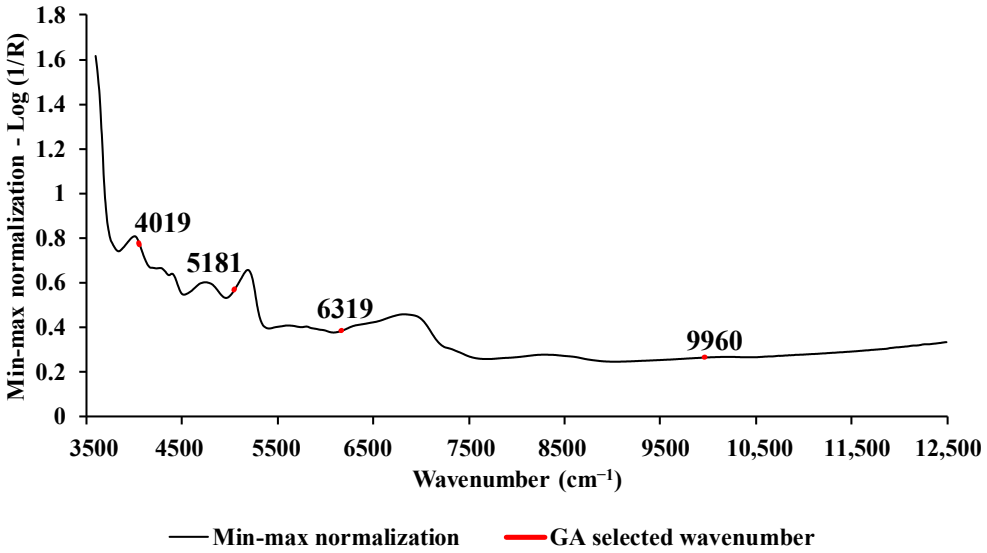

Figure 8. The average absorbance value of D_f in chip biomass using min-max normalization with selection of important wavenumbers obtained through GA.

For ground biomass, notably, as determined by R^2_P, the model performance of D_f in ground biomass has improved by 6.0322% compared to the full-PLSR approach.

Figure 9 displays the average absorbance values of D_f in ground biomass, obtained after preprocessing with D1. The figure highlights the 921 selected wavenumbers (marked in red) obtained via GA, encompassing the full spectral range of 3594.87−12,489.5 cm^{-1}. The important peaks selected at 3650, 4019, 5200, and 6897 cm^{-1} could significantly influence the model performance in evaluating the D_f in ground biomass. Table 5 presents the associated functional groups, spectra-structure, and their material types corresponding to specific peak wavenumbers observed in D_f ground biomass samples [44].

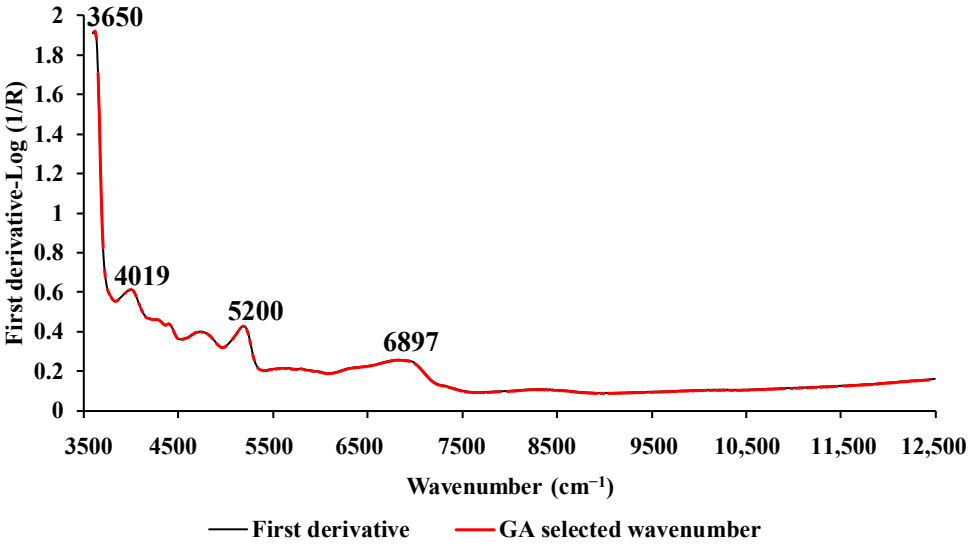

Figure 9. The average absorbance value of D_f in ground biomass using D1 with selection of important wavenumbers obtained via GA.

3.3.3. Comprehensive Combustion Index (S_i)

As shown in Table 3, the best-performing model for chip biomass was obtained through GA-PLSR with spectral preprocessing using D1, with a gap of 5 and a segment of 5 (refer to Figure 5e). By R^2 determination, the model-explained variance for S_i in chip biomass improved by 2.4712% compared to the full-PLSR method. Figure 5c shows the scatter plot of measured versus predicted S_i using GA-PLSR.

Figure 10 shows the average absorbance values of the S_i in chip biomass, obtained after preprocessing with D1. The figure highlights the 18 selected wavenumbers (marked in red) obtained through GA, covering the entire spectral range of 3595 to 12,489 cm^{-1}. Notably, important peaks were observed at wavenumbers 4019, 4292, and 7092 cm^{-1}, respectively, suggesting a potentially pivotal influence on the model's enhanced performance. Refer to Table 5, which presents the associate functional groups, spectra-structure, and the material type corresponding to specific peak wavenumbers observed in S_i chip biomass samples [44].

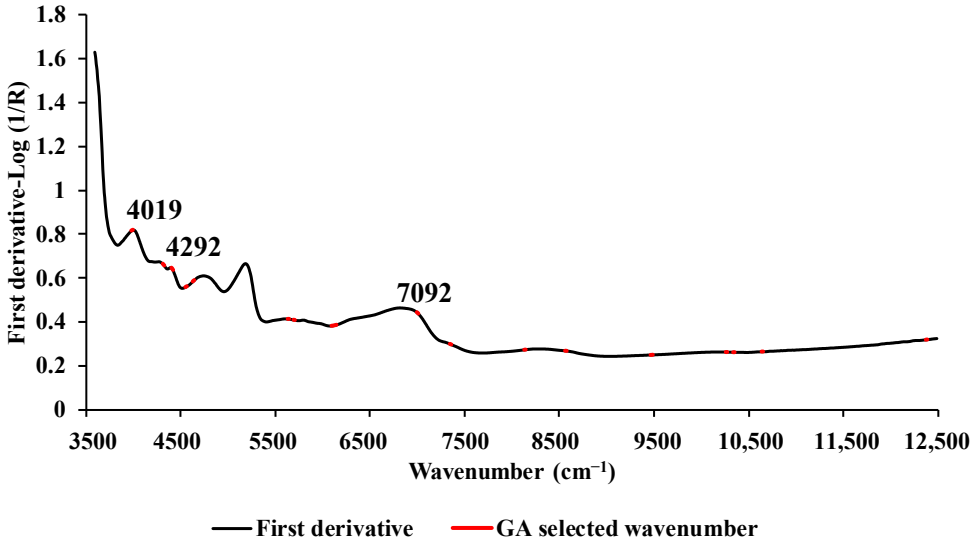

Figure 10. The average absorbance value of S_i in chip biomass using D1 with selection of important wavenumbers obtained through GA.

For ground biomass (refer to Table 4), the model performance using full-PLSR with MSC (refer to Figure 5f) as preprocessing and 14 LVs provides the best assessment for the S_i in terms of R^2_C, RMSEC, R^2_P, RMSEP, RPD, and bias. Figure 6g shows the scatter plot of measured versus predicted S_i using full-PLSR with spectrum preprocessing using MSC.

Figure 11 displays the regression coefficient for the S_i in ground biomass using full-PLSR with spectral preprocessing of MSC within the wavenumber range of 3595 to 12,489 cm^{-1}. The important peaks are noticed at 4525, 4762, 5376, 5869, 7092, and 12,300 cm^{-1}, which may significantly influence the enhanced performance of the model. Refer to Table 5, which presents the associate functional groups, spectra-structure, and the material type corresponding to specific peak wavenumbers observed in S_i ground biomass samples [44].

3.3.4. Flammability Index (C_i)

For the chip biomass model, the multi-preprocessing-PLSR with the 3-range method, employing 14 LVs and utilizing the multi-preprocessing combination set of 2, 5, 0 (i.e., SNV within the wavenumber range 3595–5493 cm^{-1}, D2 (segment = 5, gap = 5) within 7498–5500 cm^{-1}, and empty, i.e., absorbance value equals to zero, within 7506–12,489 cm^{-1}) (refer to Figure 4g), provides the best performance for assessing C_i. Figure 5d show the scatter plot of measured versus predicted C_i using the multi-preprocessing PLSR-3 range method. In addition, the model performance is improved by 8.7151% compared to the full-PLSR approach.

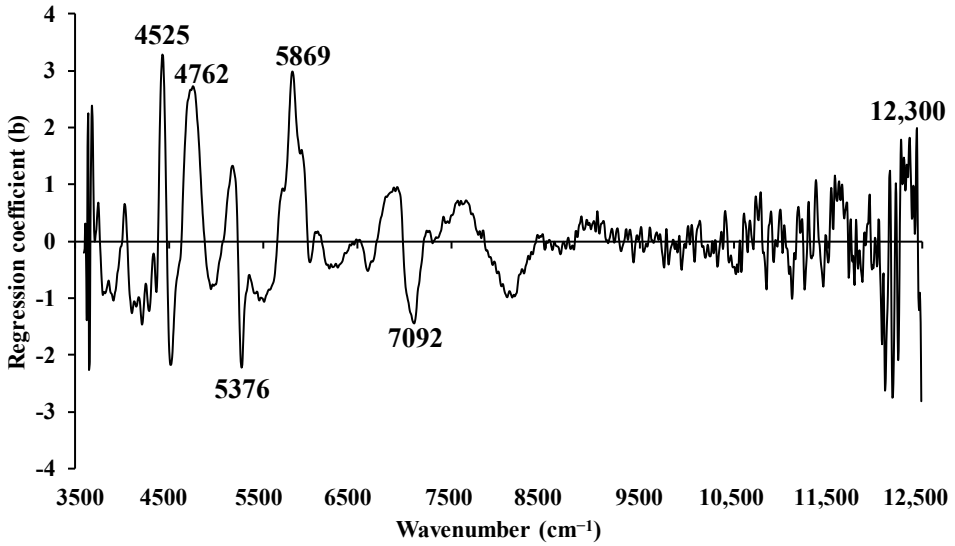

Figure 11. The regression coefficient for the S_i of ground biomass using the full-PLSR model with spectral preprocessing of MSC.

Figure 12 displays the regression coefficient for the C_i of chip biomass, utilizing the multi-preprocessing PLSR-3 range method. Notably, important peaks that might significantly influence the enhancement of the model performance are observed at wavenumbers 4202, 4307, 5241, and 5495 cm^{-1}. Within the wavenumber range of 7500–12,500 cm^{-1}, an observed regression coefficient value of zero suggests that variations in this specific variable are not associated with any changes in the predicted outcome. Table 5 presents the associated functional groups, spectra-structure, and the material type corresponding to specific peak wavenumbers observed in C_i chip biomass samples [44].

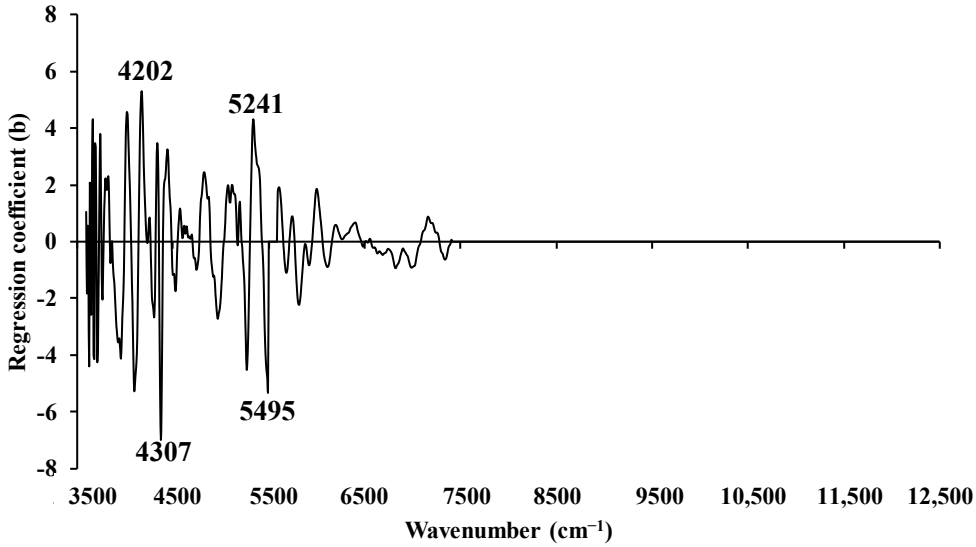

Figure 12. The regression coefficient for the C_i of chip biomass using the multi-preprocessing PLSR-3 range method with a spectral preprocessing combination set of 2, 5, 0.

From Tables 3 and 4, the overall performance of the C_i model for ground biomass is comparatively better than that for chip biomass. The best model was achieved using the multi-preprocessing PLSR-5 range method with a preprocessing combination set of 3, 2, 1, 1, 4. This combination includes the MSC from 3626 to 5392 cm^{-1}, the SNV from 5400 to 7167 cm^{-1}, raw from 7174 to 8941 cm^{-1}, raw from 8949 to 10,715 cm^{-1}, and the D1 from 10,723 to 12,489 cm^{-1} (refer to Figure 4h). Figure 5h shows the scatter plot of

measured versus predicted C_i for ground biomass using the multi-preprocessing PLSR-5 range method.

Additionally, with the multi-preprocessing PLSR-5 range method, the model performance for C_i in ground biomass improved by 4.8051% compared to the full-PLSR approach.

Figure 13 shows the regression coefficient graph for the C_i of ground biomass. This analysis utilizes the multi-preprocessing PLSR-5 range method with a spectral preprocessing combination set of 5, 0, 4, 2, and 5. Notably, significant peaks are identified at wavenumbers 5495, 5900, 6666, and 6736 cm^{-1}, which are likely to contribute significantly to enhancing the model performance in evaluating C_i within ground biomass. Table 5 presents the associated functional groups, spectra-structure, and the material type corresponding to specific peak wavenumbers observed in C_i ground biomass samples [44].

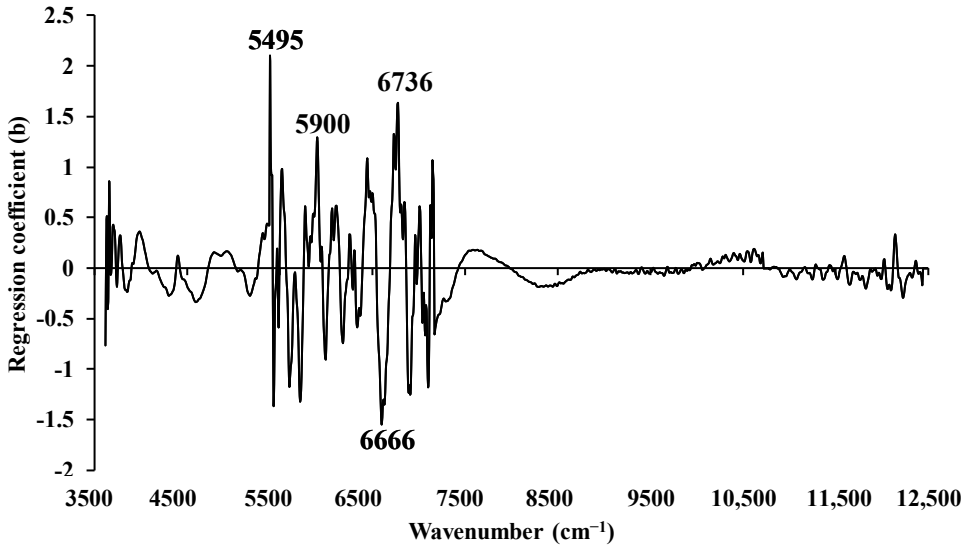

Figure 13. The regression coefficient for the C_i of ground biomass using the multi-preprocessing PLSR-5 range method with a spectral preprocessing combination set of 5, 0, 4, 2, 5.

3.4. Comparison with Previous Work

A few studies have assessed the combustion characteristic parameters and performance indices of biomass through TGA. Guohai Jia [13] previously investigated the combustion characteristics of five biomass pellet fuels using TGA at a heating rate of 20 °C min^{-1}. They calculated S_i for masson pine (1.24×10^{-8} min^{-2} K^{-3}), Chinese fir (2.28×10^{-8} min^{-2} K^{-3}), willow (7.34×10^{-9} min^{-2} K^{-3}), slash pine (5.94×10^{-9} min^{-2} K^{-3}), and poplar (1.83×10^{-8} min^{-2} K^{-3}). Shrestha et al. [45] explored the combustion characteristics of *leucaena leucocephala* pellets using TGA at a heating rate of 10 °C min^{-1}, calculating D_i, D_f, and S_i as 6.10×10^{-4} wt.% min^{-3}, 8.20×10^{-3} wt.% min^{-4}, and 2.19×10^{-7} wt.% min^{-2} $°C^{-3}$, respectively. Similarly, Shrestha et al. [46] evaluated the combustion performance indices for bamboo chips using TGA at a heating rate of 10 °C min^{-1}, deriving D_i, D_f, and S_i values of 88.33×10^{-3} wt.%.min^{-3}, 0.16×10^{-3} wt.% min^{-4}, and 3.59×10^{-7} $wt.\%^2$ min^{-2} $°C^{-3}$, respectively. The results for combustion characteristic parameters and performance indices vary across different biomass varieties due to distinct heating rates. Consequently, comparisons with previous similar biomass research may lack significance. Furthermore, to date, there have been no reports or publications on the rapid prediction of biomass combustion performance indices using NIRS for comparison.

Following William's guideline [37], if the R^2_P value falls between 0.83–0.90, the model is usable with caution for most applications, including research. For R^2_P values ranging from 0.66 to 0.81, the model can be used for rough screening and other suitable calibration purposes. For R^2_P values ranging from 0.50 to 0.64, the model is only suitable for rough to very rough screening. Following Zornoza et al. [38], any model with an RPD value below 2 is deemed insufficient for any application. If 2.0 < RPD < 2.5, it permits approximate

prediction. For 2.5 < RPD < 3, the model is considered to provide good prediction, and a value higher than 3 represents an excellent model.

According to the recommendation provided by Williams et al. [37], and based on the obtained R^2_P values, along with the consideration of RPD values, as suggested by Zornoza et al. [38], from Tables 3 and 4, we can conclude that the best models were obtained as follows: for the D_i and C_i of chip biomass, the models were suitable for rough screening, but, when considering the RPD values, they were considered insufficient for any practical applications. For the D_i and C_i of ground biomass, as well as the D_f and S_i of chip biomass, the models were considered acceptable for rough screening and certain other approximate calibrations, based on the obtained R^2_P values. However, when evaluating the RPD values, the models were inadequate for practical applications in the case of the D_i and the D_f models, providing approximate quantitative predictions for the C_i and the S_i models. The best ground biomass models for D_f and S_i can be used with caution for various applications, including research.

3.5. Benefit of Combined Agricultural Residue with Fast-Growing Trees in Model Development

Table 1 displays the range of combustion performance indices calculated for both fast-growing trees and agricultural residues, which were utilized in the development of a PLSR-based model. The analysis of Table 1 and Figure 6 reveals that agricultural residue samples exhibit a broader range in the D_i, D_f, S_i, and C_i. It is evident that the range of each combustion performance index, whether in chip or ground form, expands when agricultural residue samples are incorporated alongside samples from fast-growing trees. This broadening of the range of combustion performance indices is intended to enhance the robustness of the PLSR model for predicting combustion performance indices.

For chip biomass, apart from D_i (Figure 5a), the reference value range of D_f, S_i, and C_i (depicted in Figure 5b,c,d) in fast-growing trees was narrower compared to that of agricultural residue samples. Integrating agricultural residue samples with fast-growing trees widens their range, resulting in a comparatively enhanced model performance compared to that observed in D_i.

Similarly, concerning ground biomass, Figure 5e shows that the range of D_i for fast-growing trees is narrower than that of the agricultural residue sample. The inclusion of agricultural residue samples expanded the range, leading to better model performance compared to chip biomass. In Figure 5f, the range of D_f for fast-growing trees was higher and narrower compared to that of the agricultural residue samples. However, the inclusion of agricultural residues samples expanded the range, mostly towards the lower values, contributing to an improved model performance compared to other parameters. Likewise, Figure 5g,h illustrate that the range of fast-growing trees is narrower compared to that of the agricultural residue samples. Consequently, the inclusion of agricultural residue samples contributes to expanding the range towards both higher and lower values, ultimately enhancing the model performance.

4. Conclusions

The combustion characteristics parameters and combustion performance indices of fast-growing trees and agricultural residues were analyzed through a combined study of TG and DTG curves obtained via TGA. T_i and T_f for fast-growing trees were observed to be higher than those of agricultural residues. This suggests that fast-growing trees were harder to ignite; however, they burnt for a longer duration and produced ash more slowly compared to agricultural residues. While the calculated D_i and D_f were high for fast-growing trees, the S_i and C_i were higher for agricultural residues. This indicates that, even though agricultural residues were easier to ignite and burned more quickly and intensely (exhibiting higher thermal and combustion reactivity), their combustion processes were more controlled and less likely to experience unexpected fluctuations (better combustion stability) during thermal energy generation.

Similarly, five distinct PLSR-based models were developed and compared using NIRS to assess the D_i, D_f, S_i, and C_i under direct combustion conditions in both chip and ground biomass samples. The models with optimal performance were selected based on higher $R^2_{C,}$ R^2_P, and RPD values and lower RMSEC, RMSEP, and bias values. The results conclude that the models for D_f and S_i in ground biomass were found to be usable with caution for most applications, including research. All other combustion performance indices, both in chip and ground biomass, were suitable solely for the rough screening purpose. Therefore, a more suitable machine learning algorithm needs to be explored to improve the model performance.

The quality of reference data and spectral data, the inclusion of both agricultural residue samples and fast-growing tree samples to broaden the reference data range, proper identification of outliers, careful selection of the calibration set, and the development and evaluation of models, including spectral pre-treatment and regression methods, all play a pivotal role in establishing a reliable NIR application. Regularly updating calibration and validation procedures, including more representative samples and validating with unknown samples is crucial. Minimizing analytical errors is equally imperative for optimizing the model performance.

This research significantly contributes to the sustainable energy sector and advances our broader understanding of biomass combustion, bridging the gap between research and practical application. With its environmentally friendly behavior, the non-destructive evaluation method by NIR spectroscopy proposed in this study offers an essential and valuable alternative to traditional thermal destructive techniques, potentially revolutionizing biomass analysis. As NIR models are inherently dynamic, continual improvements and refinements in both experimental methodologies and modeling approach are essential, leading the way for future advancements to be implemented in biomass industries for both production and usage purposes.

Author Contributions: B.S.: conceptualization, methodology, software, formal analysis, investigation, resources, data curation, visualization, writing the original draft, writing—review and editing. J.P.: conceptualization, methodology, software, formal analysis, data curation, writing—review and editing, supervision. P.P.: conceptualization, methodology, writing—review and editing, and supervision. P.S.: conceptualization, methodology, data curation, writing the original draft, writing—review and editing, validation, supervision, project administration, funding acquisition. B.P.S.: conceptualization, methodology, writing—review and editing, and supervision. H.A.: writing the original draft, writing—review and editing. All authors have read and agreed to the published version of the manuscript.

Funding: This research was funded by King Mongkut's Institute of Technology Ladkrabang (KMITL), Thailand through KMITL doctoral scholarship KDS 2020/52 and The APC was partially funded by the School of Engineering, KMITL, Bangkok, Thailand.

Data Availability Statement: The data will be made available upon request from the corresponding author.

Acknowledgments: The authors would like to express their sincere gratitude to the Near-Infrared Spectroscopy Research Center for Agricultural Products and Food, the Department of Agricultural Engineering, School of Engineering at King Mongkut's Institute of Technology, Ladkrabang, Bangkok, Thailand, for their generous research funding support provided through the KMITL doctoral scholarship (KDS 2020/052).

Conflicts of Interest: The authors declare no conflicts of interest.

Abbreviations

C_i	flammability index
D1	first derivative
D2	second derivative
Di	ignition index
Df	burnout index
DTG	derivative thermogravimetric
FT	Fourier transform
GA	genetic algorithm
LV_s	number of latent variables
Max	maximum
Min	minimum
Mean	average
MSC	multiplicative scatter correction
MP	multi-preprocessing
NIRS	near-infrared spectroscopy
PLSR	partial least squares regression
R^2	coefficient of determination
R^2_C	coefficient of determination of calibration set
R^2_P	coefficient of determination of prediction set
RPD	ratio of prediction to deviation
RMSEC	root mean square error of calibration set
RMSEP	root mean square error of prediction set
S_i	comprehensive combustion performance
SD	standard deviation
SEC	standard error of calibration set
SEP	standard error of prediction set
SNV	standard normal variate
SPA	successive projection algorithm
TG	thermogravimetric
TGA	thermogravimetric analysis
T_i	ignition temperature
T_f	burnout temperature
t_i	ignition time
t_f	burnout time

References

1. IEA. Greenhouse Gas Emissions from Energy Data Explorer. Available online: https://www.iea.org/data-and-statistics/data-tools/greenhouse-gas-emissions-from-energy-data-explorer (accessed on 11 August 2023).
2. Manić, N.; Janković, B.; Stojiljković, D.; Radojević, M.; Somoza, B.C.; Medić, L. Self-ignition potential assessment for different biomass feedstocks based on the dynamic thermal analysis. *Clean. Eng. Technol.* **2021**, *2*, 100040. [CrossRef]
3. Chen, R.; Sheng, Q.; Dai, X.; Dong, B. Upgrading of sewage sludge by low temperature pyrolysis: Biochar fuel properties and combustion behavior. *Fuel* **2021**, *300*, 121007. [CrossRef]
4. Yi, Q.; Qi, F.; Cheng, G.; Zhang, Y.; Xiao, B.; Hu, Z.; Liu, S.; Cai, H.; Xu, S. Thermogravimetric analysis of co-combustion of biomass and biochar. *J. Therm. Anal. Calorim.* **2013**, *112*, 1475–1479. [CrossRef]
5. He, Y.; Chen, X.; Tang, X.; Chen, S.; Evrendilek, F.; Chen, T.; Dai, W.; Liu, J. Co-combustion dynamics and products of textile dyeing sludge with waste rubber versus polyurethane tires of shared bikes. *J. Environ. Chem. Eng.* **2023**, *11*, 109196. [CrossRef]
6. Wu, X.; Liu, J.; Wei, Z.; Chen, Z.; Evrendilek, F.; Huang, W. Oxy-fuel co-combustion dynamics of phytoremediation biomass and textile dyeing sludge: Gas-to-ash pollution abatement. *Sci. Total Environ.* **2022**, *825*, 153656. [CrossRef] [PubMed]
7. Baqain, M.; Neshumayev, D.; Konist, A. TG-MS analysis and kinetic study of co-combustion of ca-rich oil shale with biomass in air and oxy-like conditions. *Carbon Capture Sci. Technol.* **2024**, *10*, 100162. [CrossRef]
8. Demirbas, A. Combustion characteristics of different biomass fuels. *Prog. Energy Combust. Sci.* **2004**, *30*, 219–230. [CrossRef]
9. Jia, Y.; Li, Z.; Wang, Y.; Wang, X.; Lou, C.; Xiao, B.; Lim, M. Visualization of combustion phases of biomass particles: Effects of fuel properties. *ACS Omega* **2021**, *6*, 27702–27710. [CrossRef] [PubMed]
10. Gaba, A.; Iordache, S.F. Reduction of air pollution by combustion processes. In *The Impact of Air Pollution on Health, Economy, Environment and Agricultural Sources*; InTech: London, UK, 2011; pp. 119–142.

11. Alves, J.L.F.; da Silva, J.C.G.; Sellin, N.; de Borba Prá, F.; Sapelini, C.; Souza, O.; Marangoni, C. Upgrading of banana leaf waste to produce solid biofuel by torrefaction: Physicochemical properties, combustion behaviors, and potential emissions. *Environ. Sci. Pollut. Res.* **2022**, *29*, 25733–25747. [CrossRef] [PubMed]
12. Wnorowska, J.; Ciukaj, S.; Kalisz, S. Thermogravimetric analysis of solid biofuels with additive under air atmosphere. *Energies* **2021**, *14*, 2257. [CrossRef]
13. Jia, G. Combustion characteristics and kinetic analysis of biomass pellet fuel using thermogravimetric analysis. *Processes* **2021**, *9*, 868. [CrossRef]
14. Bampenrat, A.; Sukkathanyawat, H.; Seangwattana, T. *Coal/Biomass Co-Combustion Investigation by Thermogravimetric Analysis, E3S Web of Conferences*; EDP Sciences: Les Ulis, France, 2021; p. 01002.
15. Liu, J.; Jiang, X.; Cai, H.; Gao, F. Study of combustion characteristics and kinetics of agriculture briquette using thermogravimetric analysis. *ACS Omega* **2021**, *6*, 15827–15833. [CrossRef] [PubMed]
16. Idris, S.S.; Abd Rahman, N.; Ismail, K. Combustion characteristics of Malaysian oil palm biomass, sub-bituminous coal and their respective blends via thermogravimetric analysis (TGA). *Bioresour. Technol.* **2012**, *123*, 581–591. [CrossRef] [PubMed]
17. Sait, H.H.; Hussain, A.; Salema, A.A.; Ani, F.N. Pyrolysis and combustion kinetics of date palm biomass using thermogravimetric analysis. *Bioresour. Technol.* **2012**, *118*, 382–389. [CrossRef] [PubMed]
18. Cao, W.; Li, J.; Lue, L. Study on the ignition behavior and kinetics of combustion of biomass. *Energy Procedia* **2017**, *142*, 136–141. [CrossRef]
19. Lu, J.-J.; Chen, W.-H. Investigation on the ignition and burnout temperatures of bamboo and sugarcane bagasse by thermogravimetric analysis. *Appl. Energy* **2015**, *160*, 49–57. [CrossRef]
20. Arromdee, P.; Ninduangdee, P. Combustion characteristics of pelletized-biomass fuels: A thermogravimetric analysis and combustion study in a fluidized-bed combustor. *Energy Ecol. Environ.* **2023**, *8*, 69–88. [CrossRef]
21. Iryani, D.A.; Rakaseri, I.; Azhar, A.; Haryanto, A.; Hidayat, W.; Hasanudin, U. Thermogravimetric assessment for combustion characteristic of torrefied pellet biomass from agricultural solid waste. *IOP Conf. Ser. Earth Environ. Sci.* **2023**, *1187*, 012019. [CrossRef]
22. Luthfi, N.; Ohkoshi, T.; Tamaru, Y.; Fukushima, T.; Takisawa, K. Investigation into the combustion kinetics and spontaneous ignition of sweet sorghum as energy resource. *Bioresour. Bioprocess.* **2022**, *9*, 49. [CrossRef]
23. El-Sayed, S.A.; Mostafa, M.E.; Khass, T.M.; Noseir, E.H.; Ismail, M.A. Combustion and mass loss behavior and characteristics of a single biomass pellet positioning at different orientations in a fixed bed reactor. *Biomass Convers. Biorefinery* **2023**, *2023*, 1–21. [CrossRef]
24. Guo, Q.; Cheng, Z.; Chen, G.; Yan, B.; Hou, L.A.; Ronsse, F. Optimal strategy for clean and efficient biomass combustion based on ash deposition tendency and kinetic analysis. *J. Clean. Prod.* **2020**, *271*, 122529. [CrossRef]
25. Yuan, Y.; He, Y.; Tan, J.; Wang, Y.; Kumar, S.; Wang, Z. Co-Combustion characteristics of typical biomass and coal blends by thermogravimetric analysis. *Front. Energy Res.* **2021**, *9*, 753622. [CrossRef]
26. Chen, G.-B.; Li, J.-W.; Lin, H.-T.; Wu, F.-H.; Chao, Y.-C. A study of the production and combustion characteristics of pyrolytic oil from sewage sludge using the taguchi method. *Energies* **2018**, *11*, 2260. [CrossRef]
27. Posom, J.; Shrestha, B.; Maraphum, K.; Pitak, L.; Saengprachatanarug, K.; Sirisomboon, P.; Shrestha, B.P. Near-Infrared Spectroscopy, Hyperspectral, Multispectral Imaging Principles and Applications in Energy Properties of Biomass. In *A Guide to Near-Infrared Spectroscopy*, 1st ed.; Garcia Martin, J.F., Ed.; Nova Science Publishers, Inc.: Hauppauge, NY, USA, 2023.
28. Shrestha, B.; Posom, J.; Sirisomboon, P.; Shrestha, B.P.; Funke, A. Effect of Combined Non-Wood and Wood Spectra of Biomass Chips on Rapid Prediction of Ultimate Analysis Parameters Using near Infrared Spectroscopy. *Energies* **2024**, *17*, 439. [CrossRef]
29. Reza, M.S.; Taweekun, J.; Afroze, S.; Siddique, S.A.; Islam, M.S.; Wang, C.; Azad, A.K. Investigation of Thermochemical Properties and Pyrolysis of Barley Waste as a Source for Renewable Energy. *Sustainability* **2023**, *15*, 1643. [CrossRef]
30. Shrestha, B.; Posom, J.; Sirisomboon, P.; Shrestha, B.P.; Pornchaloempong, P.; Funke, A. NIR Spectroscopy as an Alternative to Thermogravimetric Analyzer for Biomass Proximate Analysis: Comparison of Chip and Ground Biomass Models. *Energies* **2024**, *17*, 800. [CrossRef]
31. Yi, B.; Chen, M.; Gao, Y.; Cao, C.; Wei, Q.; Zhang, Z.; Li, L. Investigation on the co-combustion characteristics of multiple biomass and coal under O_2/CO_2 condition and the interaction between different biomass. *J. Environ. Manag.* **2023**, *325*, 116498. [CrossRef] [PubMed]
32. Vamvuka, D.; Loukakou, E.; Avgoustidis, C.; Stratakis, A.; Pavloudakis, F.; Sfakiotakis, S. Co-combustion characteristics of lignite/woody biomass blends. Reactivity and fusibility assessment. *Energy Sources Part A Recovery Util. Environ. Eff.* **2023**, *45*, 3916–3930. [CrossRef]
33. Shrestha, B.; Posom, J.; Sirisomboon, P.; Shrestha, B.P. Comprehensive Assessment of Biomass Properties for Energy Usage Using Near-Infrared Spectroscopy and Spectral Multi-Preprocessing Techniques. *Energies* **2023**, *16*, 5351. [CrossRef]
34. Stolov, A.A.; Simoff, D.A.; Li, J. Thermal stability of specialty optical fibers. *J. Light. Technol.* **2008**, *26*, 3443–3451. [CrossRef]
35. Shrestha, B.; Shrestha, Z.; Posom, J.; Sirisomboon, P.; Shrestha, B.P. Evaluating limit of detection and quantification for higher heating value and ultimate analysis of fast-growing trees and agricultural residues biomass using NIRS. *Eng. Appl. Sci. Res.* **2023**, *50*, 612–618.

36. Maraphum, K.; Ounkaew, A.; Kasemsiri, P.; Hiziroglu, S.; Posom, J. Wavelengths selection based on genetic algorithm (GA) and successive projections algorithms (SPA) combine with PLS regression for determination the soluble solids content in Nam-DokMai mangoes based on near infrared spectroscopy. *Eng. Appl. Sci. Res.* **2022**, *49*, 119–126. Available online: https://ph01.tci-thaijo.org/index.php/easr/article/view/245217 (accessed on 28 December 2023).
37. Williams, P.; Manley, M.; Antoniszyn, J. *Near Infrared Technology: Getting the Best out of Light*; African Sun Media: Stellenbosch, South Africa, 2019.
38. Zornoza, R.; Guerrero, C.; Mataix-Solera, J.; Scow, K.M.; Arcenegui, V.; Mataix-Beneyto, J. Near infrared spectroscopy for determination of various physical, chemical and biochemical properties in Mediterranean soils. *Soil Biol. Biochem.* **2008**, *40*, 1923–1930. [CrossRef] [PubMed]
39. Xue, J.; Yang, Z.; Han, L.; Chen, L. Study of the influence of NIRS acquisition parameters on the spectral repeatability for on-line measurement of crop straw fuel properties. *Fuel* **2014**, *117*, 1027–1033. [CrossRef]
40. Madhu, P.; Dhanalakshmi, C.S.; Mathew, M. Multi-criteria decision-making in the selection of a suitable biomass material for maximum bio-oil yield during pyrolysis. *Fuel* **2020**, *277*, 118109. [CrossRef]
41. Cardarelli, A.; Pinzi, S.; Barbanera, M. Effect of torrefaction temperature on spent coffee grounds thermal behaviour and kinetics. *Renew. Energy* **2022**, *185*, 704–716. [CrossRef]
42. Brassard, P.; Palacios, J.H.; Godbout, S.; Bussières, D.; Lagacé, R.; Larouche, J.-P.; Pelletier, F. Comparison of the gaseous and particulate matter emissions from the combustion of agricultural and forest biomasses. *Bioresour. Technol.* **2014**, *155*, 300–306. [CrossRef]
43. Mansora, A.M.; Lima, J.S.; Anib, F.N.; Hashima, H.; Hoa, W.S. Characteristics of cellulose, hemicellulose and lignin of MD2 pineapple biomass. *Chem. Eng.* **2019**, *72*, 79–84.
44. Workman, J., Jr.; Weyer, L. *Practical Guide to Interpretive Near-Infrared Spectroscopy*; CRC Press: Boca Raton, FL, USA, 2007.
45. Shrestha, A.; Saechua, W.; Sirisomboon, P. Some physical and combustion characteristic of Leucaena Leucocephala pellet. In Proceedings of the 16th TSAE National Conference and 8th TSAE International Conference, Agricultural and Food Engineering Outlook on Sustainable Future, ET-08, Bangkok International Trade & Exhibition Centre, Bangkok, Thailand, 17–19 March 2015; pp. 127–132.
46. Shrestha, A. *Feasibility Study on Near Infrared Spectroscopy for Evaluation of Combustion Performance Parameters and Moisture Content of Bamboo Chips (Dendrocalamus Sericeus cl. Phamon)*; King Mongkut's Institute of Technology: Ladkrabang, Thailand, 2016.